Dry Metal Forming Open Access Journal

Final Project Report

Edited by Frank Vollertsen
Available online at https://elib.suub.uni-bremen.de

www.drymetalforming.de

Dry Met. Forming OAJ FPR 6 (2020) 228–261
Date of Report 31 May 2020; published 12 June 2020

Lubricant free forming with tailored tribological conditions

(DFG Grant No. ME 2043/43&50; SCHM 2115/36&49; TR 1043/1&5; Funding Period 01.04.2014 – 31.07.2020)

Johannes Henneberg*[1], Benedict Rothammer[2], Rong Zhao[2], Martin Vorndran[3,4], Jennifer Tenner[1], Kim Krachenfels[1], Tom Häfner[3,4], Stephan Tremmel[2], Michael Schmidt[3,4], Marion Merklein[1]

[1]Institute of Manufacturing Technology, Friedrich-Alexander-Universität Erlangen-Nürnberg (FAU), Egerlandstr. 13, 91058 Erlangen, Germany
[2]Institute of Engineering Design, Friedrich-Alexander-Universität Erlangen-Nürnberg (FAU), Martensstr. 9, 91058 Erlangen, Germany
[3]Institute of Photonic Technologies, Friedrich-Alexander-Universität Erlangen-Nürnberg (FAU), Konrad-Zuse-Str. 3/5, 91052 Erlangen, Germany
[4]Erlangen Graduate School in Advanced Optical Technologies (SAOT) Friedrich-Alexander-Universität Erlangen-Nürnberg (FAU), Paul-Gordan-Str. 6, 91052 Erlangen, Germany

Summary

Changed ecological and economic situations motivate research into environmentally friendly and efficient manufacturing processes. Forming without lubricant has the potential to meet both requirements by avoiding the usage of environmentally harmful lubricants and shortening the process chain by omitting lubricant application and component cleaning. Within the scope of the project, an increase in friction and adhesive wear were identified as major challenges, resulting in failure of components due to cracking. Therefore, this project focused on the investigation of measures to meet these challenges. Amorphous carbon coatings, the reduction of roughness and the application of discrete microtextures were considered as potential measures. Hydrogen-containing amorphous carbon coating systems (a-C:H) fabricated by reactive physical vapor deposition (PVD), plasma-enhanced chemical vapor deposition (PECVD) and PVD/PECVD hybrid techniques, as well as a PVD-generated tetrahedral hydrogen-free amorphous carbon coating (ta-C) were investigated with respect to their properties and tribological performance Three specific profile requirements – a dopant free carbon network, smooth and defect-free surfaces and a high coating adhesion to substrate – are identified as requirements, in order to prolonger the service life of the coated tools. Moreover, to enable the steering of the material flow ultrafast laser based micro texturing for locally tailored tribological conditions were investigated. Thereby two wavelength dependent ablation regimes which differ in ablation mechanism and freedom of form were identified. Using these approaches the friction coefficient could either be reduced by up to 20 % or selectively increased. To improve the efficiency of the process, several beam shaping approaches were evaluated to provide a homogeneous beam profile for uniform modification. By applying ta-C and a-C:H coatings in forming tests, the findings of the laboratory tests were validated and the feasibility of lubricant free deep drawing was proven. In order to benefit from the forming-process-specific advantages, high quantities and therefore high durability of the measures are required. An application-oriented wear test rig has been designed to investigate their durability. By this, it was proven that 3 000 components can be produced from DC04 without wear with both a-C:H and ta-C coatings, and thus increasing tool life by a factor of 15 compared to unmodified tools. Even in the case of wear-critical AA5182, 3 000 parts were produced without wear using ta-C. Within the scope of the project, a fundamental understanding of lubricant free deep drawing processes and measures was created and proof of feasibility in form of a high number of components was achieved.

Keywords: Dry Deep Drawing, Tribology, Carbon Based Coatings, Laser Based Surface Modification, Beam Shaping

*E-mail address of corresponding author: johannes.henneberg@fau.de

1 Introduction and methodology

Sheet metal forming is a widespread manufacturing technology which is used in large-scale productions, for example in the automotive industry, as well as in small series, for instance in aircraft production [1]. The economically most important process of sheet metal forming is deep drawing [2]. The usage of lubricants to reduce friction and tool wear as well as to improve component quality is widespread. The lubricant, which is often based on mineral oils, is applied to the semi-finished products before forming and must be removed by chemical cleaners after forming prior to further processing steps. In this context, both economic reasons, such as shortening the process chain by omitting the application of lubricant and cleaning, as well as for ecological reasons, such as the omission of environmentally harmful lubricants and cleaners, motivate dry forming [3]. Based on this vision, the objective was the realization of dry deep drawing processes using tailored forming tools. The lubricant is to be replaced by a local or global adaptation of the tool surfaces with coating systems and laser-based texturing. To achieve this objective, the approach shown in Fig. 1 was chosen.

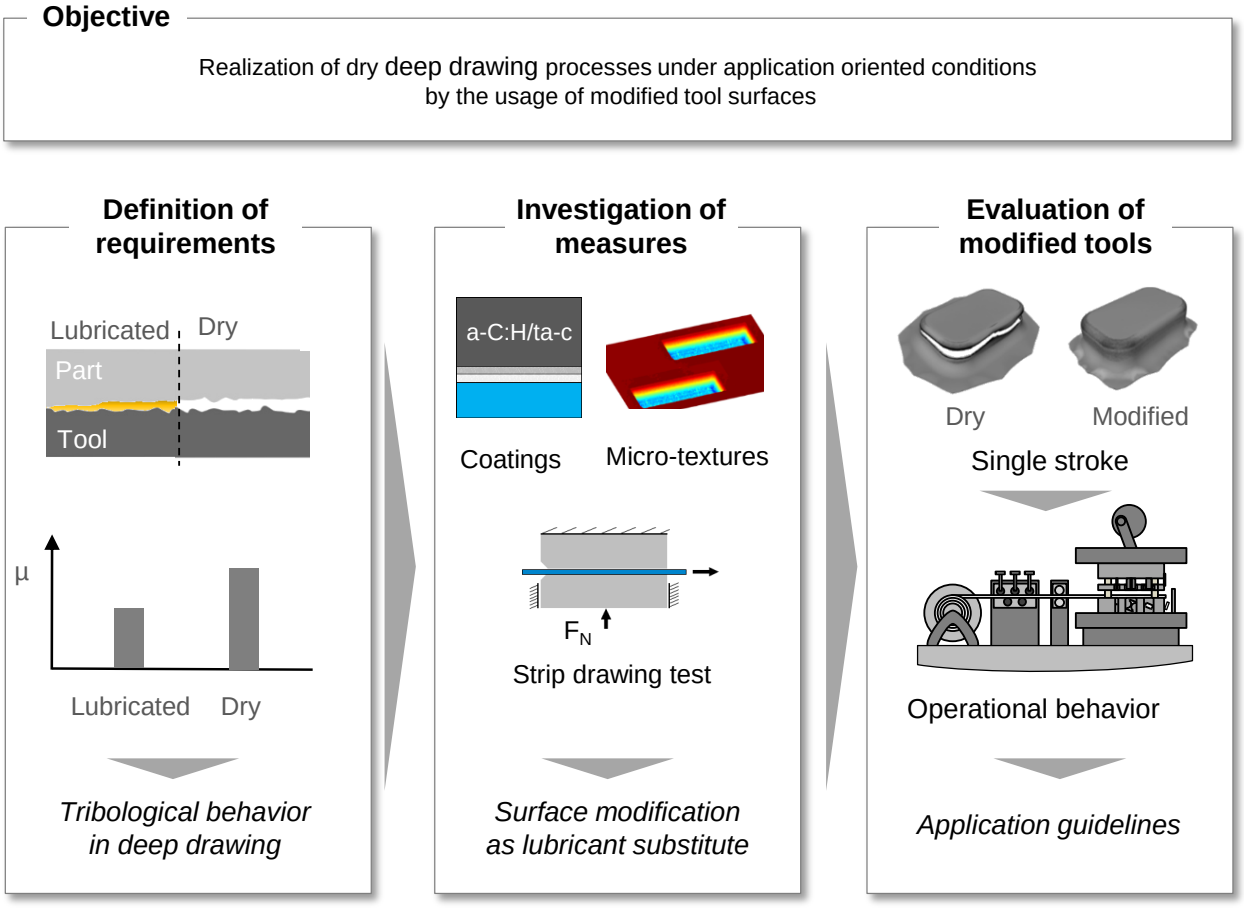

Fig. 1: Objective and methodology

In a first step, a fundamental insight into the lubricant free deep drawing processes was obtained. By analyzing the effects of the omission of lubricant on the tribology, the requirements for the measures were derived. For this purpose, the relationship between friction and wear was determined in a combined numerical-experimental approach and the dominant wear mechanisms were investigated. Based on this knowledge, measures to meet the challenges were researched. For doing so, the functional relationships between coating topography, chemical composition of the coating and friction as well as wear were determined in the abstract laboratory tests flat strip drawing and flat strip bending rotation. Using this knowledge as a basis, it was researched how to adjust the coating process in order to achieve advantageous coating properties. Besides the coatings, textures have the potential to adjust the tribological conditions

locally and therefore enable the possibility to steer the material flow in dry deep drawing. For texturing the surface an ultrafast laser is chosen due to its ability for cold ablation, which enables to adjust the topography without changing the chemical composition of the heat sensitive coating. The knowledge gained from the laboratory tests, in combination with the requirements defined in the first step, enabled the choice of suitable surface modifications. In a final step, these were evaluated in forming processes to verify the findings. For this purpose, forming processes were designed and tools with modified surfaces were used. For an economic production, a high service life of the forming tools is necessary. A new test rig was developed to investigate the wear behavior of the modified tools and used for the production of 3 000 components per measure. Finally, by combining the central findings of the project, recommendations for the design of dry deep drawing processes were derived, thus creating an important basis for the reduction of lubricant usage in industrial deep drawing.

2 Materials and investigated surface modifications

2.1 Materials

In order to investigate dry deep drawing, the mild steel DC04 (1.0338) is applied as the workpiece material, which is well established for complex component geometries [4]. To ensure the transferability of the findings, the aluminum alloys AA5182 (EN AW-Al Mg4,5Mn0,4) and AA6014 (EN AW-Al Mg0,6Si0,6V) are utilized as additional materials. AA5182 is often applied for structural components in the automotive industry [5]. All sheets have an electro discharged textured (EDT) surface and a thickness of 1 mm. The steel material is coated with zinc for corrosion protection. Knowledge of the mechanical material properties is of great importance for numerical investigations and as an explanation for materials' tribological behavior. For this purpose, a material characterization was conducted as shown in Fig. 2.

For the evaluation of the mechanical material properties tensile tests, biaxial tensile tests and Nakajima tests were performed. From these tests, the yield surface modelled according to Barlat 2000 was derived [6], see Fig 2 a). The yield surface represents the transition from elastic to plastic material behavior. The DC04 yield surface has the largest shape, meaning that DC04 requires the highest stresses for deep drawing. The lowest stresses are required for AA5182. Flow curves were determined for all materials based on tensile test and are illustrated in Fig. 2 b). They were measured experimentally up to a true strain of maximum 0.2. Since higher true strains are necessary for the forming simulation, the flow curves were subsequently extrapolated up to a true strain of 1.0 according to the Hockett-Sherby approximation, which is commonly used in sheet metal forming [7]. From the flow curves it can be seen that all materials harden up to a degree of true strain of 0.4 and then show an almost constant strength level. At approximately 400 MPa, DC04 has a higher yield stress than the aluminum alloys with 330 MPa or respectively 350 MPa. The forming limit curve (FLC), see Fig. 2 c), was also determined as the basis for the numerical mapping of the material behavior. If the combination of main and minor strain exceeds the curve, component failure occurs in the form of cracks. An almost identical behavior is determined for the aluminum alloys. In contrast, the steel alloy DC04 has a significantly higher forming limit curve. With the determined data, the mechanical behavior of the materials can be numerically reproduced and thus, dry deep drawing processes can be numerically investigated. In addition, a difference in the mechanical properties was identified. The selection of the materials is therefore suitable for testing the transferability of the findings to materials with different mechanical properties.

The tool material used for all investigations was tool steel X155CrVMo12 (1.2379) with a hardness of 60 ± 2 HRC. In metal forming, fine machining of the tool surfaces to reduce friction and wear by polishing or lapping is established [8]. Therefore, all tools were mechanically polished to a mean roughness Rz of 0.2 ± 0.1 µm and a reduced peak height R_{pk} of 0.05 ± 0.02 µm.

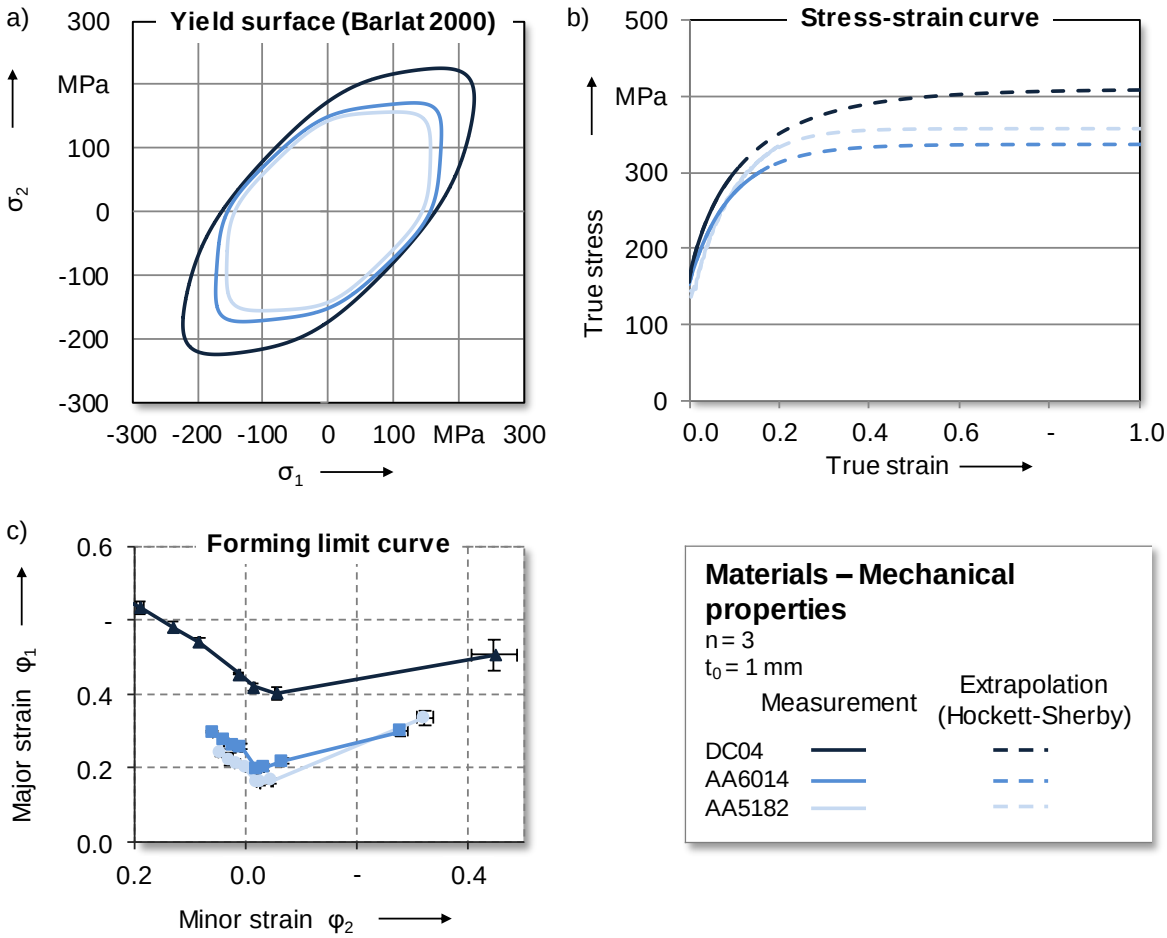

Fig. 2: Mechanical properties of workpiece materials: a) yield surface, b) stress-strain curve and c) forming limit curve

2.2 Surface modifications

PVD and PECVD are vacuum deposition processes to produce high-performance coatings. They are often applied to deposit thin coatings on bulk materials [9], so that mechanical properties, tribological behavior as well as physical and chemical surface characteristics can be adjusted. The substrates are cost-efficient materials (e. g. steel) and the coatings can bring new functions or modifications with desired properties. The coating architecture, deposition technologies and deposition parameters can be controlled by programming the deposition recipe [10]. In this project, both of the mentioned vacuum deposition technologies are used to fabricate the amorphous carbon coating systems on tool surfaces. Amorphous carbon coatings, also called diamond-like carbon (DLC) coatings, are well known for their excellent tribological performance [11] and are considered here as a replacement for the lubrication. The amorphous carbon coatings have a unique chemical structure: It consists of both sp^2 and sp^3 as well as rare sp^1 bonded carbon atoms [12]. This unique structure makes amorphous carbon coatings attractive in tribological uses with a lubricated effect from sp^2 bonded atom rings on the one hand and with high hardness from sp^3 hybridized atoms on the other hand [13].

3 Definition of requirements: Research on the tribology of dry deep drawing

In order to develop a fundamental knowledge as well as to determine the requirements for the measures for the realization of dry deep drawing processes, the tribology of dry and lubricated deep drawing has to be compared. In a first step, abstracted laboratory tests were used to investigate friction and wear. Based on these findings, the feasibility of dry deep drawing processes is then examined numerically and requirements for measures are derived.

3.1 Development of laboratory tests

For the analysis of friction the flat strip drawing test is used. This test is widely used to analyze the friction occurring during deep drawing [14]. The test parameters and the test set-up applied in the research project are described in [15]. By this test setup the tribological conditions in the flange area are reproduced. For deep

drawing, the die radius is the highly loaded area [16]. In order to reproduce this area as well, the strip bending rotation test shown in Fig. 3 was developed within the scope of the project.

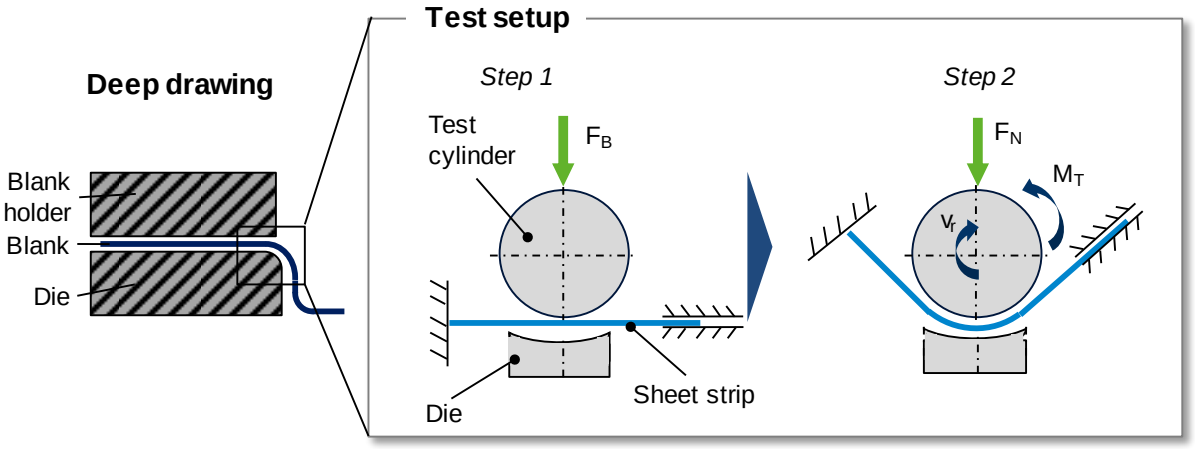

Fig. 3: Principle of strip bending rotation test

In a first step of this test, a metal strip is clamped with the bending force F_B between the die and a test cylinder representing the die radius of deep drawing tools. After clamping, the material-specific normal force F_N is applied to reproduce the numerically determined tribological conditions at the drawing ring. Thus, contact pressures of 22 MPa are set for the material DC04 and 12 MPa for the aluminum alloys. The test cylinder is then rotated by 90° at a defined speed v_r of 36 mm/s. The necessary rotational torque M_t is measured and the coefficient of friction μ is determined according to Coulomb's law of friction based on the normal force F_N and the torque M_t. Compared to flat strip drawing, this test setup allows the mapping of higher tribological loads and thus a more realistic representation of the conditions at the drawing ring radius. Additionally, in strip drawing, failure would occur in the form of tearing of the strips under the high contact pressures. Besides, the bending and friction forces are easier to separate in this test setup.

3.2 Experimental analysis of friction and wear

For the analysis of dry forming, strip drawing tests and bending rotation tests were conducted with non-lubricated workpieces, while lubricated parts were used as a reference. In the flat strip drawing test, the absence of lubricant causes a substantial increase in friction from a low level between 0.03 and 0.05 to 0.15 for DC04, 0.30 for AA5182 and 0.57 for AA6014, see Fig. 4 a). The slight increase in DC04 compared to the aluminum alloys is due to the topographies of the workpieces. All parts have an EDT surface, with DC04 additionally coated by zinc. In addition, the reduced peak height R_{pk} before forming is lowest for DC04 at 0.41 ± 0.05 µm and highest for AA6014 at 1.68 ± 0.18 µm. Consequently, the effect of mechanical interlocking of roughness peaks dominates in AA6114 and the increase in friction is more distinct compared to DC04. The influence of the parameters contact pressure and relative velocity was investigated in detail in [15]. No significant influence was found for the dry state, as there is no lubricating film, which changes depending on the process parameters. The comparison of the friction in the dry state in the flat strip drawing test and in the strip bending rotation test in Fig. 4 b) gives a good agreement of the results, although there are different process parameters such as relative velocity and higher contact pressure during bending rotation test. This confirms the finding that in dry deep drawing the process parameters have a minor influence on friction. Nevertheless, in the lubricated state the friction coefficients are higher in the strip bending rotation test than in the flat strip drawing test. This is due to the lower relative velocity and higher surface pressure. According to Stribeck's curve, this results in a thinner level of the lubricant film. A comparable behavior was found in [17]. The analysis of the friction jaws after the five tests, see Fig. 4 c), shows clear signs of wear for the aluminum alloys. In [16] the wear was identified as adhesion. Aluminum is adhering to the friction jaws and is then sheared off by the relative movement between tool and workpiece. In [18], this wear mechanism was also identified for the strip bending rotation test. The strongest wear occurs with the alloy AA6014 and is presumably due to the high reduced peak height of the material texturing.

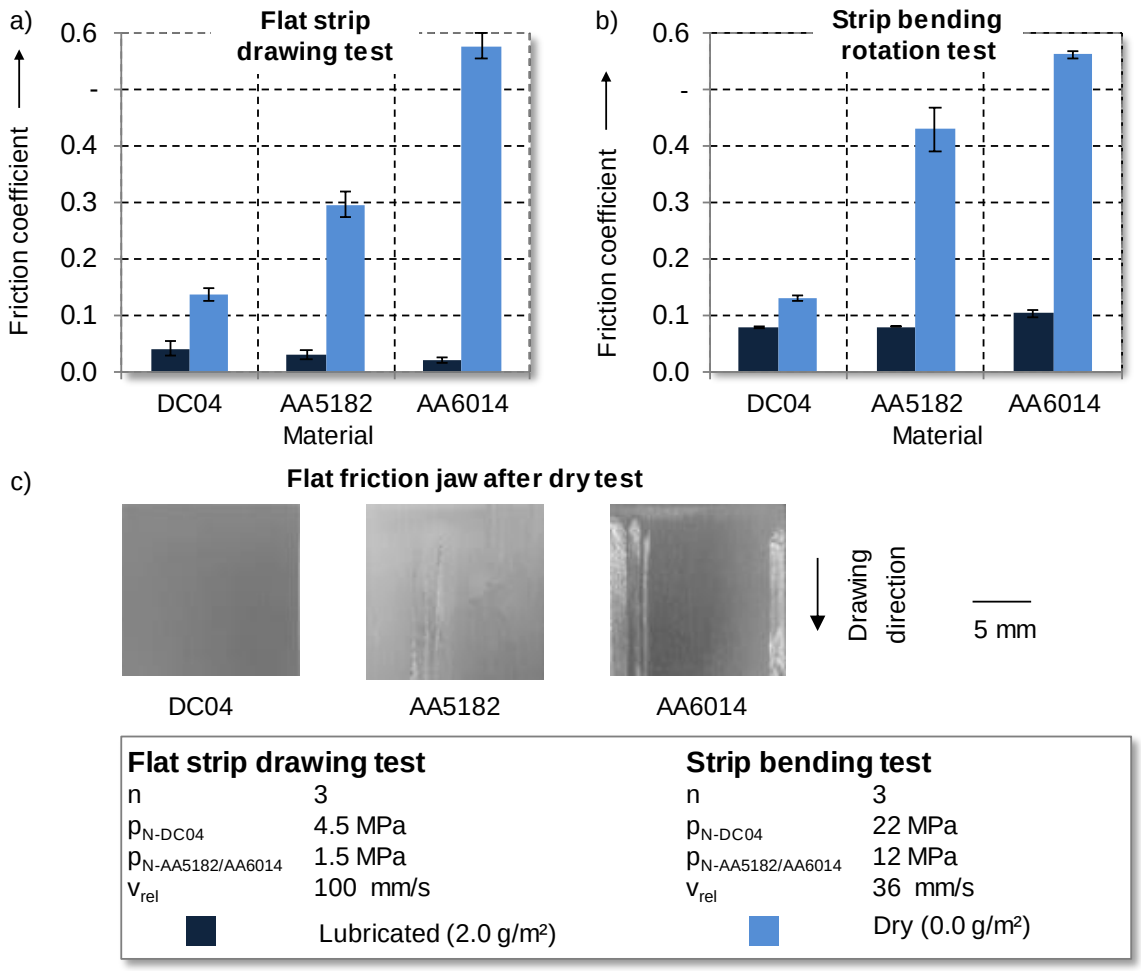

Fig. 4: Friction and wear in a) flat strip drawing and b) strip bending rotation test as well as c) friction jaws after dry tests

Based on the findings of the laboratory tests, a distinct increase in friction and adhesive wear were identified as the central challenges of dry deep drawing. The increase in friction is critical, as high friction during deep drawing can cause cracking of the components. The wear impairs the quality of the workpiece surfaces and additionally increases friction. Consequently, the influence of lubricant removal on deep drawing processes is numerically analyzed in the following and the requirements for measures to overcome these challenges are derived.

3.3 Numerical analysis of dry deep drawing

In order to investigate the influence of the challenges identified in section 3.2 on forming processes, a deep drawing process has been designed, see Fig. 5, in which a blank with a defined geometry is deep drawn into a rectangular cup with a size of 53 mm to 93 mm. The aim of this process is, on the one hand, to determine the effects of the omission of lubricant on the forming process and, on the other hand, to define the requirements for the modifications to realize lubricant free deep drawing processes. A numerical model was built to investigate the process. The model is described in [15] and was validated in [19] for AA6014 and in [20] for DC04 and AA5182. The key requirements for modifications to realize lubricant free deep drawing processes are the prevention of adhesive wear and the reduction of friction to avoid component failure in the form of cracks.

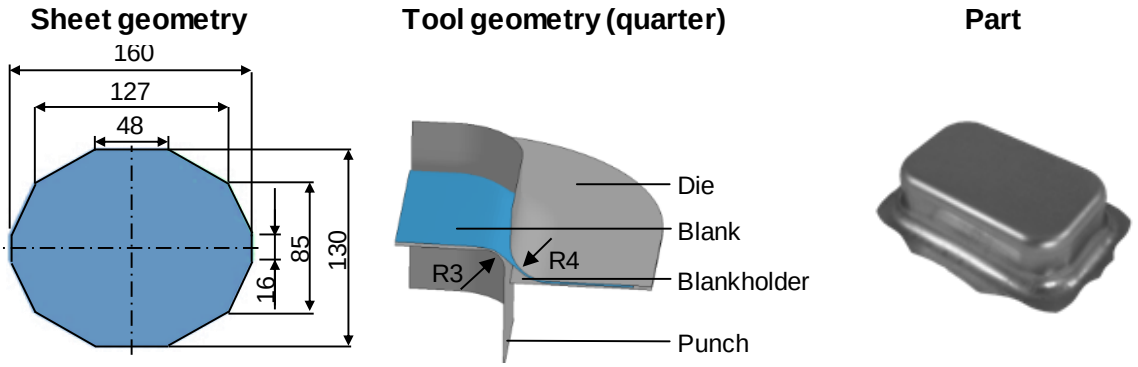

Fig. 5: Experimental setup of deep drawing process

In order to identify the friction level that has to be achieved by the modifications, variant simulations were conducted. For this purpose, the friction for all materials was varied in 0.05 steps from 0.05 as friction in a lubricated case to the friction identified in section 3.2 for dry forming without modification. By analyzing the strain paths and comparing them with the FLC of the materials, it can be evaluated which friction is necessary for failure-free forming. The major and minor strain for DC04 at a friction coefficient of 0.2 are as illustrated in Fig. 6 a) below the FLC. Therefore, no failure by cracking is expected even in lubricant free case. Consequently, the main requirement for the modifications when forming DC04 is to prevent wear, which would negatively influence the component surface quality. In case of the aluminum alloys, see Fig. 6 b) and Fig. 6 c), the major strains exceed the FLC and the minor strains are close to zero when forming without modification. Thus, it can be assumed that tensile stress dominates and the material flows out of the sheet thickness, which results in local sheet thinning and cracks. Only a reduction in friction to 0.3 reduces the strains to an uncritical level. For the lubricant free forming of AA5182 and AA6014 the modifications should consequently reduce friction to a level of maximum 0.3 in addition to the prevention of wear. Thus, in the next two sections measures to meet these requirements are investigated.

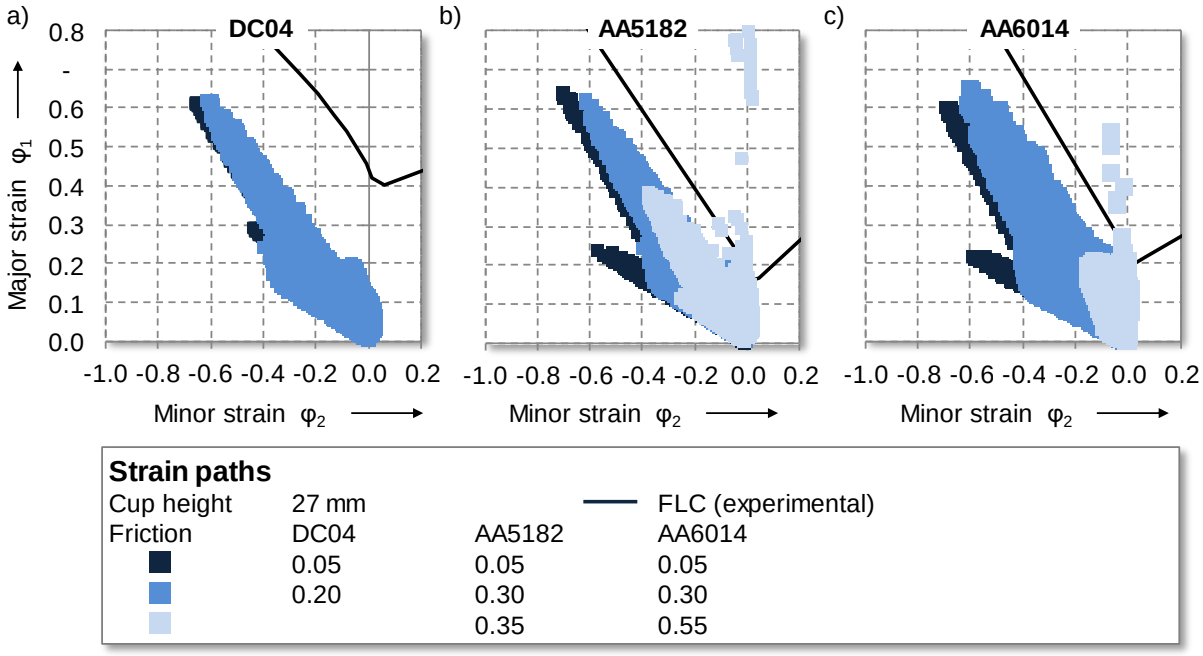

Fig. 6: Strain paths at a drawing depth of 27 mm for varying friction coefficients in accordance to [20] for a) DC04, b) AA5182 and c) AA6014

4 Tribologically optimized amorphous carbon coatings

From the laboratory tests, adhesion is identified as the dominant wear mechanism during the dry deep drawing process. In this project, two kinds of amorphous carbon coating systems with different predominating C-C bond types [21], a-C:H and ta-C, are considered as solutions to affect the intensive tribological interactions during dry forming. With the application of an amorphous carbon coating system on the forming tool surface, reduction of friction and prevention of the metallic adhesive wear are desired. The

a-C:H coating system is well known for its tribological application and can be fabricated with low production costs and machine investments. The properties of a-C:H coatings can be adjusted over a wide range, since the deposition process can be realized by (plasma enhanced) CVD with different carbonaceous gases (e. g. acetylene [22], methane [23]) as well as by reactive PVD sputtering of a graphite target. The ta-C coating with dominant sp^3 boned carbon atoms has extreme high hardness and thus is also suitable as wear protection coating on forming tools [24].

The investigations of coating systems on forming tools is carried out according to the methodology described in Fig. 7. It consists of two main parts considering the previously specified two coatings variants. The a-C:H coatings are investigated by varying coating designs and parameters as well as chemical composition by doping metallic elements. The aim is to produce a coating system with high adhesion strength to the tool substrate and provide beneficial tribological conditions for dry forming process. Furthermore, correlations between each varied parameter and coating properties are shown. The ta-C coating is produced by an industrial partner with standard ta-C coating system for industrial uses. The tribological performance of the deposited coating systems against aluminum alloys and steel is evaluated in flat strip-drawing test. According to the resulted wear and observed friction behavior after the tribological laboratory tests, the coatings with lowest wear and friction against metal sheets are selected for forming tools and evaluated their service life in mass production.

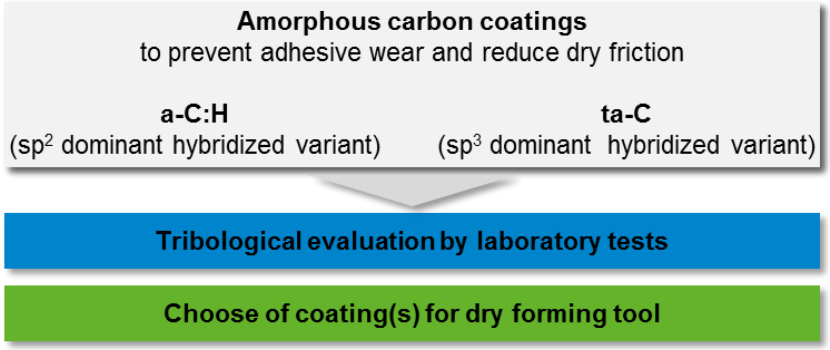

Fig. 7: Investigation process of amorphous carbon coatings for dry forming tools

4.1 Hydrogenated amorphous carbon coatings (a-C:H)

As mentioned before, adhesion and metallic material transfer are considered as the dominating wear mechanisms in dry contact with sheet metals, especially in contact with aluminum alloys. In order to improve the friction conditions and prevent adhesive wear, a-C:H coatings are applied on tool surfaces. The investigated a-C:H coatings were deposited using a hybrid PVD/PECVD coating machine (H-O-T, TT 300) with a twofold rotating charging rack. Fig. 8 illustrates the cross section of the applied standard a-C:H coating system. For a high adhesion to the steel substrate, a chromium (Cr) adhesive layer, a tungsten carbide (WC) interlayer and an a-C:H:W gradient layer were deposited prior to a-C:H functional layer according to DIN 4855 [25]. Intermediate layer(s) of WC and a-C:H:W ensure gradient material change from adhesive layer to functional layer. The mechanical processing and cleaning procedures of the steel substrate and the deposition process of Cr/WC/a-C:H:W-layers prior to the functional layer are documented in [26]. Characterization methods for coating thickness, hardness and adhesion to the substrate are mentioned in [26].

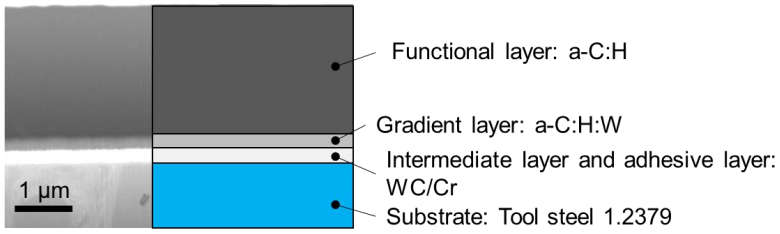

Fig. 8: Standard a-C:H coating architecture

Effect of deposition parameters on coating properties

For a systematic investigation of a-C:H coatings for dry sliding use, a pre-evaluation of possible parameters, which affect the coating properties, was conducted. Many factors can affect the final features of a-C:H

coatings and their tribological performance, which cover from precursor gas species, existence of sputter gas, gas pressure, substrate bias voltage, reactor temperature, to previous etching, heating processes and even contaminations in the reactor. These parameters affect the coating properties differently. These different coating properties have direct or indirect impacts on wear mechanisms and influence the friction conditions. The friction conditions affect the wear behavior, like loose particle occurrence and adhesion accumulation between tool and workpiece. Essential parameters, which affect the deposition process of the a-C:H functional layer are chosen and their effects on coating properties are investigated.

First, the precursor gas, process pressure and sputter gas will be investigated systematically. The a-C:H coating samples are deposited each at varied C_2H_2/Ar ratios ranging from 1:1 to 5:1 and varied total gas flows of C_2H_2+Ar from 200 sccm and 300 sccm. The detailed deposition parameters and sample preparation are summarized in [27]. Main effect plots of the gas ratio and the total gas flow on coating properties are shown in Fig. 9. As shown in Fig. 9 a), the deposition rate increases with C_2H_2 concentration if the coatings have been deposited with a gas flow of 300 sccm. The C-H radicals attached more quickly to the substrate boundary surface than the other atoms in the reactor [28]. Therefore a higher concentration of C_2H_2 accelerates the coating growth process. It can also be seen that the deposition rate for 200 sccm was very low and almost unaffected by gas composition. Due to the low total flow and thus low pressure in the PECVD reactor, the glow discharge of gases was performed with a lower current. The ions and radicals in this plasma field did not gain enough kinetic energy and therefore did not enhance coating growth. Fig. 9 b) shows that the effect of adhesion depends strongly on total gas amounts. As shown in Fig. 9 c), the effect of gas ratio on hardness of the coatings is not very pronounced considering large standard deviation. As Fig. 9 d) indicates, the deposition rate increases with the process gas amount. The higher amount of total gas atoms in the reactor accelerates the formation of clusters and thus the growth of coatings [29]. Fig. 9 e) shows that the a-C:H coating deposited under higher process pressure has generally better adhesion. However, hardness decreases with rising gas amounts (see Fig. 9 f)). The same effect is observed if the total flow increases. According to [30], increasing C_2H_2 flow led to a reduction of hardness and indentation modulus in a WC-doped a-C:H-matrix, as the C_2H_2 amount varied from 0 to 10 sccm. The investigation conducted in [10] shows the same tendency, as the C_2H_2 amount varied from 7 to 49 sccm. In plasma with low total gas amounts the mean free path of each molecule is longer and thus leads to less energy loss through collision with other species. Ions with high energy promote the formation of sp^3 bond formations [31], which is associated with high hardness and indentation modulus. However, it fits reasonably with sp^3-rich and hard amorphous carbon coatings like ta-C, but less so for a-C:H [32]. In the case of a-C:H coatings the hardness depends more on the form of existing sp^2 bonded carbon atoms, which is discussed with the help of RAMAN data in [27].

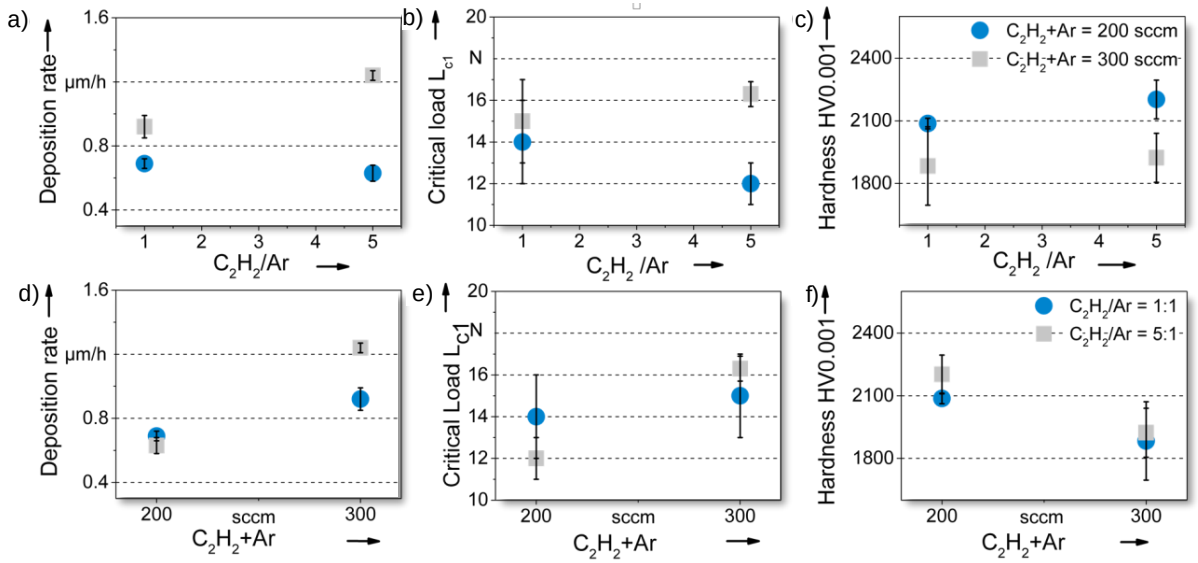

Fig. 9: Main effect plots of gas ratio on a) deposition rate, b) critical load of the first crack L_{c1}, and c) hardness HV0.001 and main effect plots of total gas flows on d) coating deposition rate, e) critical load of the first crack L_{c1} and f) hardness HV0.001 (n=2, each effect point is gained from two data at two levels)

Besides of the reaction gas atmosphere, the substrate bias voltage and the deposition temperature, which are also associated with mechanical properties of the coatings, are investigated using one-factor-at-a-time

experimentation. The process temperature has great impact on the coating structure and growth procedure. In the coating growth model according to [33], the coating structure was found to become denser and more crystalline as the substrate temperature increases. Furthermore, an increasing temperature results in reduction of compressive residual stress and thus better adhesion [34]. The negative bias voltage is well known for its impact on coating properties such as hardness and growth rate [35]. Thus, the coating properties, which are associated with the tribological behavior under dry sliding conditions, are possible to be specifically adjusted by varying the bias voltage.

The a-C:H coating samples are deposited under the same conditions as these for the variation of gas precursors. For the present experiment, acetylene and argon were remained generally constant at 166 sccm and 34 sccm, respectively, since a higher total gas amount or lower C_2H_2/Ar ratio results in reducing in hardness. The temperature was investigated over the range of 80 °C to 140 °C with a constant bias voltage of 550 V. The highest level of 140 °C was chosen as the same temperature for depositing the WC-interlayer. The lowest factor level of 80 °C was selected, because the substrates are stored at this temperature in the vacuum oven before the coating process. The bias voltage was adjusted over a wide range from 450 V to 950 V, in which a stable deposition process was ensured. In this case, the temperature was kept constant at 80 °C. The level of 950 V was chosen since a higher bias voltage led to over-heating of the substrate, e. g. a voltage of 1 200 V led to an actual deposition temperature of 120 – 130 °C although the nominal temperature was set to 80 °C.

The a-C:H functional layers deposited at 80 °C to 140 °C have a thickness of 2.3 µm to 2.5 µm. As Fig. 10 a) indicates, no relationship was observed between deposition rate and temperature. All the coating samples deposited at varied temperatures have an adhesion of HF4, which represents a sufficient adhesion with small cracks and delamination around the ROCKWELL indent according to [36]. Fig. 10 b) reveals the micro hardness of coated samples deposited at varied temperature. The average hardness HV(H_{IT})0.001 values increase slightly with the temperature. Samples deposited at 120 °C and 140 °C show higher standard deviations of hardness than those deposited at lower temperatures. Fig. 10 c) shows that the coating thickness increased with bias voltage. The energy-rich ionic species at higher bias voltages supported the growth process. The growth rate per every increased 100 V is flatterned because the effect of increasing bias voltage up to an extreme high value of 950 V by surface bombardment must be considered. Another observed side effect is over-heating of the substrate, e. g. the measured actual reactor temperature was around 90 °C – 100 °C if the bias voltage was set to 950 V, which was 10 °C to 20 °C higher than the nominal temperature of 80 °C. A bias voltage of 450 V leads to better adhesion of the coating system to the substrate of HF3, while other coating systems show adhesion class of HF4. Average hardness is shown in Fig. 10 d). As the bias rises from 450 V to 700 V, the hardness increases. Due to the strong bombarding effect at 950 V, the growing coating was etched, and a homogenous coating and adhesion to substrate could not be ensured. Consequently, the sample at 950 V shows a reduced hardness.

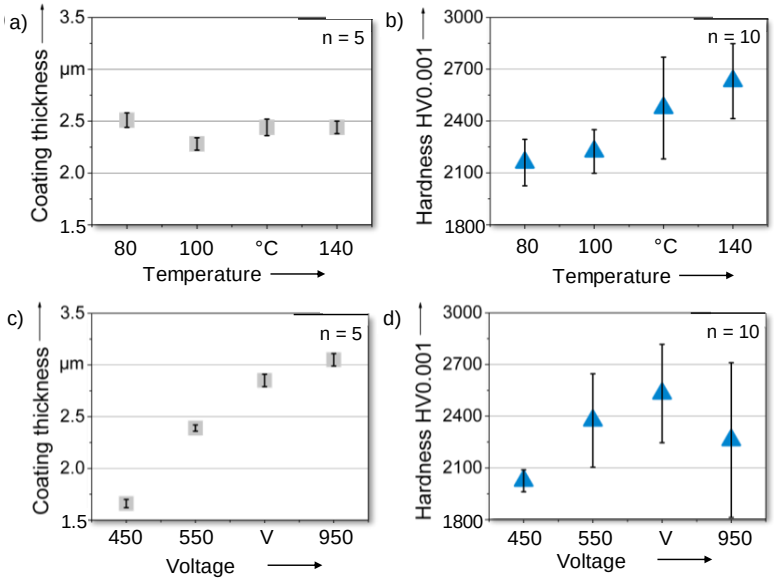

Fig. 10: Relationships between a) coating thickness and temperature, b) hardness and temperature, c) coating thickness and bias voltage and d) hardness and bias voltage

In Fig. 11, the surface topography and their height information of coating samples deposited at different conditions are shown. Comparing Fig. 11 a) and b), more coating defects began to grow on the surfaces with increasing temperature. From their height information in Fig. 11 d) and e), these obvious defects on the surface deposited at high temperature are cavities and cracks. This inhomogeneous coating surface in Fig. 11 b) and e) also results in great fluctuations in hardness. As mentioned before, higher process temperature leads to denser coatings [33], which explains the increased hardness shown in Fig. 10 b). Considering Fig. 11 a) and c), higher bias voltage lead to obviously denser coating surface with little surface defects.

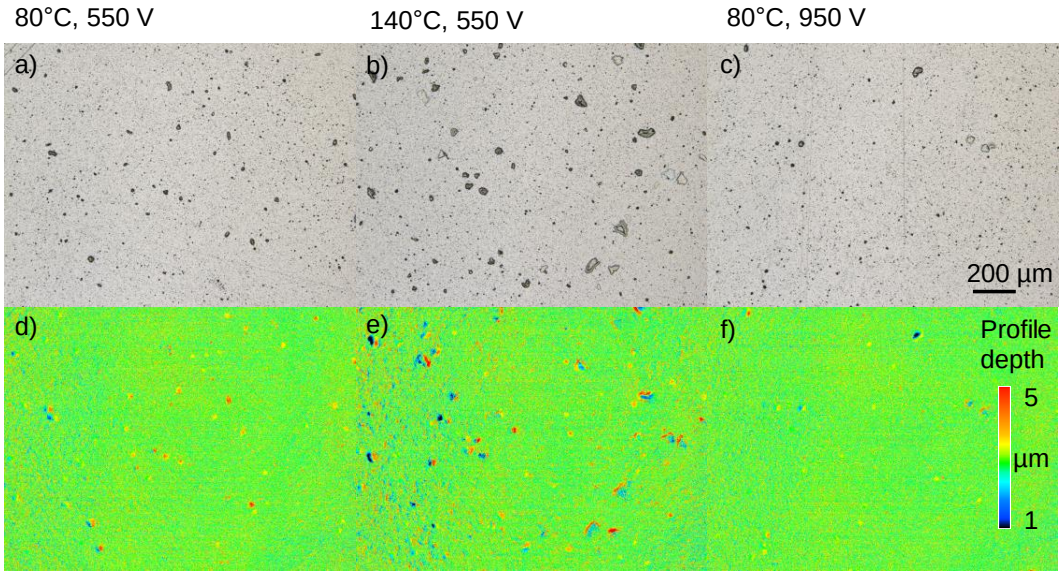

Fig. 11: Surface topography of the coating sample at a) low temperature and low bias voltage, b) high temperature and low bias voltage and c) low temperature and high bias voltage; height information of coating surface at d) low temperature and low bias voltage, e) high temperature and low bias voltage and f) low temperature and high bias voltage

Generally, the gas amount or process pressure has greater effect on the essential coating properties than that of acetylene concentration, since the amount of gas affects strongly the kinetic energy of the gas species in the reactor. Both, substrate temperature and bias voltage influence the mechanical properties and the coating structure. A higher temperature results in a more inhomogeneous and brittle coating structure, which leads to spalling after polishing. The ionic species under high bias voltage with high energy accelerate the coating growth process. However, side effects including surface etching and over-heating above 700 V cannot be avoided.

Coating architecture and deposition technologies

Besides the deposition parameters, roughness, mechanical properties and chemical bond structures of the a-C:H coating system have great impact on the dry sliding behavior. These three parameters can be modified by changing the coating architecture through multilayers and by changing deposition technology. As Fig. 12 illustrates, different modifications of the standard a-C:H coating system are investigated with the aim to adjust certain parameters, which affects the tribological behavior under dry conditions. Modification of the mechanical properties of the a-C:H coating system is realized by changing the functional layer with multilayer design. The aim is to investigate the effect of hardness-to-elasticity ratio on tribological performance without changing the top layer. Chemical composition in the amorphous carbon network is modified by doping metallic elements. Its adhesion tendency of the doped amorphous carbon coatings to aluminum alloy in dry contact is evaluated and compared with non-doped variant. The chemical bond structures of the a-C:H coating system is varied by changing the deposition technology. Instead using PECVD the a-C:H can also be deposited by magnetron sputtering of a graphite target in C_2H_2-Ar-atmosphere. The a-C:H coating system in as-deposited state shows high roughness and cannot be used for applications due to severe abrasive wear, especially in dry sliding contact. The roughness is reduced by changing the deposition technology of the Cr adhesive layer.

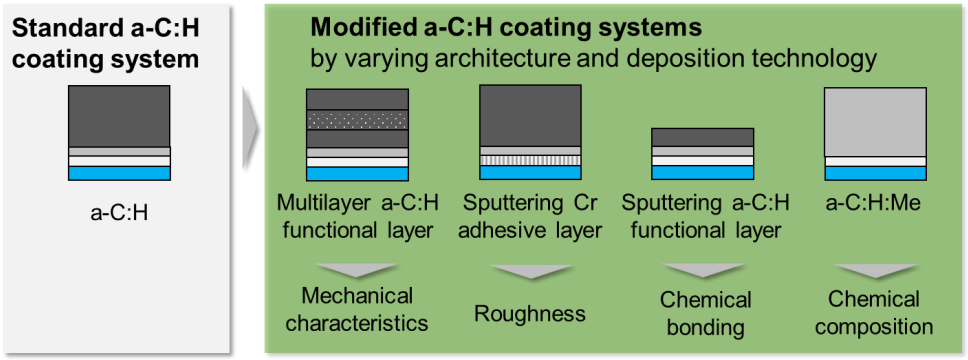

Fig. 12: Overview of investigated modified a-C:H coating systems by varying architecture and deposition technology

The multilayer functional coating includes three monolayers with the sequence of a-C:H/a-C:H:SiO/a-C:H. The layer thickness of the a-C:H/a-C:H:SiO/a-C:H sequence was adjusted in such a way that the functional layer thickness of the standard coating system was not exceeded. Tab. 1 summarized the detailed deposition parameters each for a-C:H and a-C:H:SiO layers.

Tab. 1: Detailed deposition parameters for standard a-C:H coating layer and the a-C:H:SiO intermediate layer for multilayer design

	Bias voltage/V	Power supply	Temperature/°C	C_2H_2/sccm	Ar/sccm	HMDSO/sccm
a-C:H functional layer	450	40 kHz, pulse width 5 µs	100	220	40	0
a-C:H:SiO intermediate layer						10

The properties of both coating systems are listed in Tab. 2. The a-C:H multilayer has slightly lower coating thickness and better coating adhesion. The H_{IT}/E_{IT} ratio of the multilayer system is slightly higher than that of the monolayer system, which indicates, that this deposited multilayer variant is considered more ductile than that the monolayer variant.

Tab. 2: Comparison of the standard a-C:H coating system and its multilayer variant

Coating properties	Unit	Monolayer a-C:H	Multilayer a-C:H/a-C:H:SiO/a-C:H
Deposition time for functional layer	s	7 200	2 400/2 000/2 400
Thickness of the functional layer (n = 5)	µm	1.98 ± 0.02	1.60 ± 0.02
Indentation hardness H_{IT} (n = 5)	GPa	23.6 ± 3.0	20.3 ± 2.6
Indentation modulus E_{IT} (n = 5)	GPa	203.8 ± 21.0	166.8 ± 17.5
H_{IT}/E_{IT}	-	0.116	0.122
Adhesion (n = 5)	-	HF4	HF3

The Cr adhesive layer in the standard a-C:H coating system was deposited by vacuum arcing. This is the reason, why the deposited a-C:H surface is very rough in the as-deposited state, since a large amount of droplets is formed during the vacuum arc process. Therefore, a modified coating system was developed in which the Cr adhesive is sputtered. The detailed deposition parameters for both coating systems are summarized in Tab. 3.

Tab. 3: Detailed deposition parameters for Cr adhesive and a-C:H functional layers each in standard and modified system

Cr adhesive layer ↓	Deposition time/s	Power supply	Energy input	Ar flow/sccm	T/°C
Basic Cr adhesive layer by vacuum arcing	520	-	70 A	70	140
Modified Cr adhesive layer by magnetron sputtering	520	70 kHz, pulse width 4 µs	5 000 W	130	140
a-C:H functional layer ↓	**Deposition time/s**	**Bias voltage/V**	**C_2H_2 flow/sccm**	**Ar flow/sccm**	**T/°C**
Basic a-C:H coating system	8 580	450	220	40	100
Modified a-C:H coating system	8 580	550	220	40	80

Sputtering the Cr adhesive layer leads to a much lower surface roughness of the coating than that by vacuum arcing, so that the post-polishing of the coating surface can be omitted or shortened. [37] Fig. 13 reveals the

surface topography of both coating systems. By sputtering the Cr adhesive layer, a more homogenous coating surface with less defects is produced. Both coating systems have an adhesion class of HF3.5 according to Rockwell C indentation test. However, sputtering the Cr adhesive layer leads to significant reduction of the critical load for initial substrate exposure L_{c3} from 33.4 N to 23.4 N [37], which implies that the coating adhesion becomes weaker by sputtering the Cr adhesive layer.

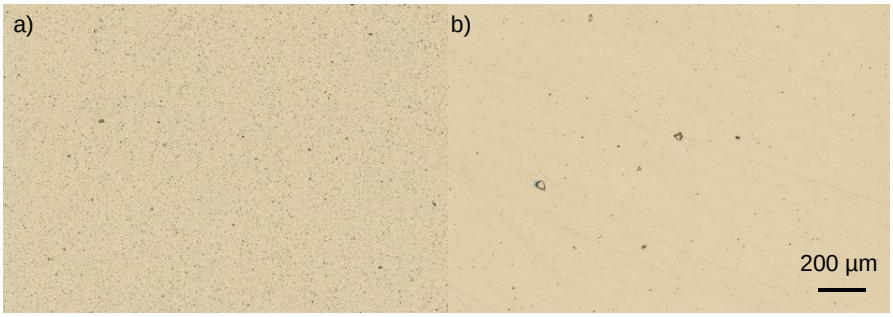

Fig. 13: a-C:H coating surfaces with a) arced Cr adhesive layer and b) sputtered Cr adhesive layer

The a-C:H functional layer was as well produced by magnetron sputtering of a graphite target with the aim to investigate the effect on chemical bonds by changing deposition technology and source material. The detailed deposition parameters are listed in Tab. 4.

Tab. 4: Detailed deposition parameters for a-C:H by PECVD and sputtering, respectively

	Bias voltage/V	Power supply	Energy input	Temperature/°C	C_2H_2/sccm	Ar/sccm
a-C:H by PECVD	450	40 kHz, pulse width 5 µs	-	100	220	40
a-C:H by magnetron sputtering	200	70 kHz, pulse width 4 µs	1 000 W	100	20	200

Tab. 5 summarized the properties of both coating systems. The deposition rate of the a-C:H coating fabricated by magnetron sputtering of a graphite target is much lower than that of the a-C:H coating fabricated by PECVD in C_2H_2-Ar-atmosphere. Both coatings have similar H_{IT}/E_{IT} ratio of about 0.12. The sputtered a-C:H functional layer has a thinner coating thickness compared to the PECVD a-C:H functional layer and thus lower residual stresses, which leads to a slightly better adhesion of the layer to the substrate. Both coating samples are analyzed with Raman spectroscopy, which is suitable for the non-destructive analysis of amorphous carbon. The sputtered a-C:H coating has lower I_D/I_G ratio and higher $FWHW_G$ value, which implies that the coating has a high sp^3/sp^2 ratio. [32]

Tab. 5: Comparison of the standard a-C:H functional layer by PECVD and modified functional layer by magnetron sputtering

Coating properties	Unit	a-C:H by PECVD	a-C:H by magnetron sputtering
Deposition time	s	8580	8580
Deposition rate (n = 5)	µm/h	0.8	0.1
Indentation hardness H_{IT} (n = 10)	GPa	17.5 ± 1.0	24.1 ± 3.3
Indentation modulus E_{IT} (n = 10)	GPa	137.9 ± 5.7	194.8 ± 18.6
H_{IT}/E_{IT}	-	0.127	0.124
Adhesion (n = 5)	-	HF4	HF3
Intensity ratio of D and G peak I_D/I_G*	-	1.7	1.1
Peak width at half height of G peak $FWHW_G$	cm^{-1}	157.6	187.2

*Equivalent to area ratio of D and G peaks if using Gauss function

The metal-doped amorphous carbon coatings (a-C:H:Me) are considered as one of the other coating modifications that may reduce the friction. Within this project, a tungsten doped hydrogenated amorphous carbon coating (a-C:H:W) was deposited by reactive unbalanced magnetron sputtering of a binder-free WC target using a medium frequency power supply in an argon-acetylene atmosphere. The a-C:H:W coating system has the same architecture and adhesive layers as the standard a-C:H coating system. In addition, an a-C:H:(W:Mo)S_x coating was also fabricated for further reducing dry friction. It was deposited using magnetron sputtering of both a WC target and a MoS_2 target. The adhesive and intermediate layers are applied in the same way as described in Fig. 8 for standard a-C:H coating system. The parameters for

sputtering WC were chosen analogously. Tab. 6 summarized the deposition parameters for the both coating systems.

Tab. 6: Detailed deposition parameters for a-C:H:W and a-C:H:Me

	Energy input	Bias voltage/V	Power supply	Temperature/°C	C_2H_2/sccm	Ar/sccm
a-C:H:W	1 400 W for WC target	130	40 kHz, pulse width 5 µs	100	220	180
a-C:H:(W:Mo)S_x	1 000-2 000 W for MoS_2 target	57-203	40 kHz, pulse width 5 µs	100	20	128-232

The metal-doped variant a-C:H:Me has generally the highest adhesion strength to substrate with adhesion class of HF1. However, the hardness of the a-C:H:Me is only 40 % of the undoped a-C:H coating system, since the basic carbon network is destructed by introducing large tungsten (W) and Molybdenum (Mo) atoms.

In summary the coating properties, which are associate with dry sliding behavior, are adjustable by varying architectural coating design and deposition technology. Modifications of chemical composition and bonds are realized mainly by changing deposition technology and source material. Mechanical properties more tend to be modified by architectural design. A wide process window of H/E ratio can be realized by varying layer number and layer thickness or even change the intermediate layer. However, the modifications may bring change in coating adhesion and deposition rate, which must be controlled before the practical application.

4.2 Tetrahedral amorphous carbon (ta-C)

As illustrated in Fig. 14, the ta-C coating system consists of an adhesive layer of Cr and the ta-C functional layer. For a smooth coating surface, the Cr adhesive layer is sputtered. The ta-C layer was deposited applying the pulsed-laser arc process, which is initiated by a laser pulse on the graphite target. In order to ensure a smooth coating surface, a magnetic field is used to filter macro particles from the particle stream. After deposition, the coated samples are polished and brushed with diamond paste with a grain size of 3 µm. The ta-C coating contains over 85 % of sp^3 hybridized carbon according to the supplier. Due to its high fraction of diamond-like carbon bonds (sp^3-bonds) the ta-C coating exhibit extremely high hardness and wear resistance. The detailed properties of ta-C coating are summarized in Tab. 7.

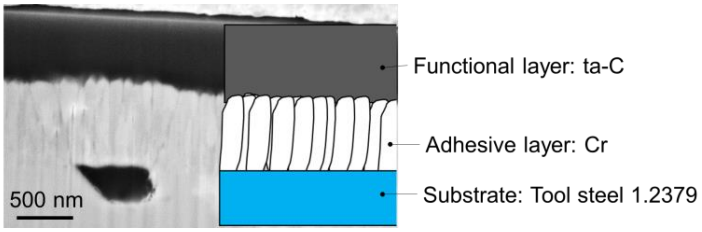

Fig. 14: Architecture of tetrahedral amorphous carbon coating (ta-C)

4.3 Tribological evaluation of coatings in laboratory test

Investigated amorphous carbon coatings for tribological testing and their basic properties are summarized in Tab. 7. Characterization methods and test parameters for measuring coating thickness, hardness and adhesion strength are mentioned in previous investigations according to VDI 2840 [21].

Tab. 7: Essential properties of ta-C, standard a-C:H and modified a-C:H coating systems

Designation	Coating thickness in µm	Hardness H_{IT} in GPa	Indentation modulus E_{IT} in GPa	HF class
ta-C [41]	1.3 ± 0.1*	54.6 ± 7.1	330.6 ± 52.4	HF2
a-C:H:W [42]	2.4 ± 0.1	6.9 ± 1.6	86.1 ± 7.5	HF1
a-C:H [42] (standard)	1.8 ± 0.1	17.5 ± 1.0	137.9 ± 5.7	HF3.5
a-C:H (sp-Cr interlayer) [38]	2.6 ± 0.1	17.0 ± 0.7	131.6 ± 5.0	HF3.5
a-C:H (sp-graphite) [25]	0.6 ± 0.0	24.1 ± 3.3	194.8 ± 18.6	HF3
a-C:H/a-C:H:SiO/a-C:H [25]	2.8 ± 0.0	20.3 ± 2.6	151.8 ± 17.5	HF3

*Thickness determined by cross-section with focused ion beam (FIB), while other samples with calotte grinding method

Prior to tribological tests, all the coating samples are post-treated by polishing. The deposited coating system has higher roughness asperities than that of the steel substrates. Due to this high roughness the coating in as-deposited state cannot be applied directly for dry sliding, as it causes high abrasive wear and high friction. For the coating system on forming tools the coating surfaces are mechanical post-treated by polishing with a soft cloth or diamond suspension with 1 µm. Investigations on the relationship between the reduced peak height R_{pk} and the coefficient of friction showed, that a lower R_{pk} value on ta-C coated surface led to a lower friction, especially during sliding against aluminum alloys. [38] If the hard amorphous carbon tips interlock with the ductile and textured aluminum sheet, the risk of initial metal transfer rises and the service life of tools is shortened.

The surface modifications in Tab. 7 are evaluated in strip-drawing test under dry sliding conditions. Fig. 15 a) shows that the coefficients of friction against steel sheet DC04 are generally low, independent of the surface modifications. The reason is the corrosion protective zinc film on the DC04 sheet surface, which leads to low friction and low adhesion tendency. Fig. 15 b) reveals that the friction against aluminum alloy depends strongly on the surface modifications. The a-C:H:W coating shows 300 % higher friction in dry contact with the aluminum alloy compared to the ta-C coating. The a-C:H:W coating has a columnar structure from the growth process [10], which leads to an inhomogeneous and cauliflower-like surface topography. Even after polishing, the ductile aluminum alloy is sheared through the edges of micro-textures and the initial adhesion storage in the valley on the surface. In addition, the element tungsten leads to high adhesion tendency in direct contact with aluminum. [39] Thus, the aluminum tends to stick onto the a-C:H:W coated surface. The a-C:H and ta-C coated friction jaws show 30 % and 50 %, respectively, lower friction against aluminum alloys than uncoated steel. The lower friction can be explained in two aspects. First, they have a certain percentage of sp^3 hybridized carbon bonds. Even the a-C:H coatings, which are deposited from an acetylene-argon gas mixture, have 20 % – 40 % percentage of sp^3 bonds [40], which prevents the adhesion and benefits the friction. However, no linear relationship between the percentage of sp^3 bonds and friction was found: the a-C:H coating with lower sp^3 ratio shows a similarly low friction as the ta-C coating. The second important reason is the low R_{pk} value, which reduces the risk of the formation of initial aluminum adhesion. As shown in Fig. 15 b), the modified a-C:H coating system by sputtering a Cr adhesive layer with a homogeneous surface shows a little lower friction against AA5182 than that of the standard a-C:H system. However, the polishing cannot be omitted, as otherwise the resulted friction is two times higher than that of the treated surfaces. It can be seen, that the a-C:H coating system with sputtered a-C:H functional layer has a little lower friction than that of the standard coating system. The multilayer design has however higher friction.

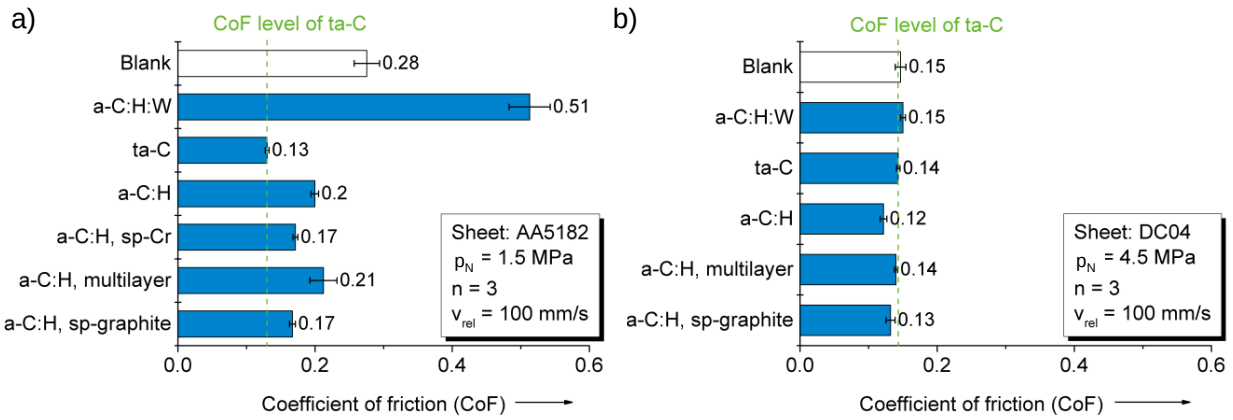

Fig. 15: Coefficient of friction in strip drawing test against a) steel sheet DC04 and b) aluminum alloy AA5182 under dry sliding condition

The worn surface was analyzed with confocal microscopy. From Fig. 16 it can be seen that metallic transfer was found on the steel and a-C:H:W test jaws. On the a-C:H and ta-C surfaces there are no obvious adhesions.

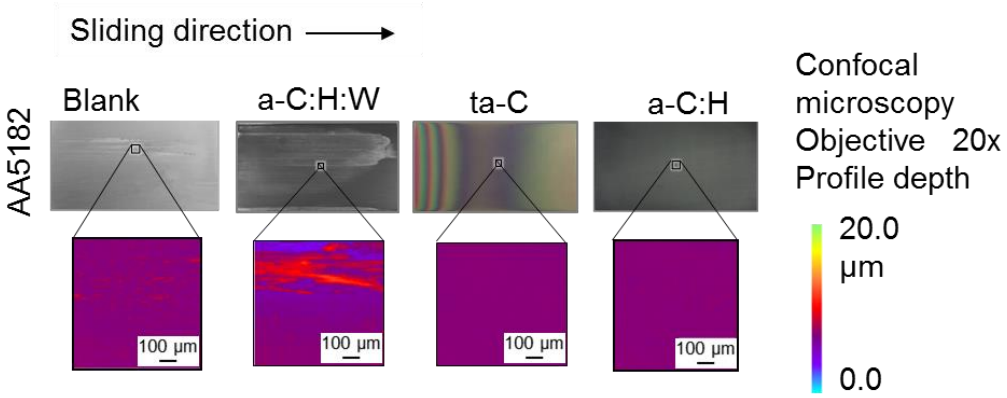

Fig. 16: Analysis of worn surfaces of steel, a-C:H:W, ta-C and a-C:H coatings

The simple laboratory tests show that the dominated wear mechanism between tool steel and aluminum alloy is metal transfer. To realize dry metal forming, adhesion from sheet material to tool surface should be avoided. The ta-C coatings show low friction and the tested surface shows no adhesion or other material residues. Besides the ta-C coating, the a-C:H coating system shows similar low friction as the ta-C coating. Compared to the ta-C coatings, the a-C:H coatings deposited in acetylene-argon atmosphere are easy to produce concerning low machine investment and production costs, which makes its application on tool surface attractive. Therefore, the a-C:H and the ta-C coatings are selected for further application-related durability tests.

5 Laser based surface texturing and modification

In addition to the coating, micro textures and their possibility of changing the friction coefficient are evaluated. The ability of locally changing the friction coefficient can be used to create a segmented tool and therefore allow the steering of the material flow in dry deep drawing. To successively develop the necessary knowledge of the tribological effect of micro textures and the ultrafast laser based surface treatment of DLC coatings the following steps were performed.

Laser texturing of flat, uncoated steel was evaluated in a first step to determine how micro textures influence directly the tribological conditions on metallic bright surfaces. These results were then used as a starting point to investigate structuring of flat, coated surfaces, but before that also ultrafast laser polishing of these surfaces was developed. The findings from the flat surfaces were then applied to curved geometries which mimic the conditions of deep drawing in the flange area.

Finally, to improve the surface treatment in terms of efficiency and therefore create the basis for the economic usability of ultrafast laser based surface treatment different beam shaping techniques were investigated and compared.

5.1 Surface texturing of uncoated 1.2379 steel surfaces

To evaluate the possibility of tailoring the friction coefficient by micro textures, bright metallic surfaces were textured with an ultrafast laser and then strip drawing tests were performed to mimic the conditions of the deep drawing process. The generation of the micro features is explained in detail in [41]. The micro features on the uncoated tool have a depth of 5 µm and a rectangular shape with a width of 500 µm and a length of 100 µm. A degree of surface coverage of 10 % showed the best wear behavior for a blank metallic textured surface [41]. The results of the strip drawing tests with DC04 under dry conditions are shown in Fig. 17 a). For both surfaces, a relatively low friction with μ varying between 0.14 and 0.15 is measured without any significant improvement by texturing. Although the friction coefficient cannot be reduced significantly, the structuring is still beneficial due to its function as reservoir for wear particles.

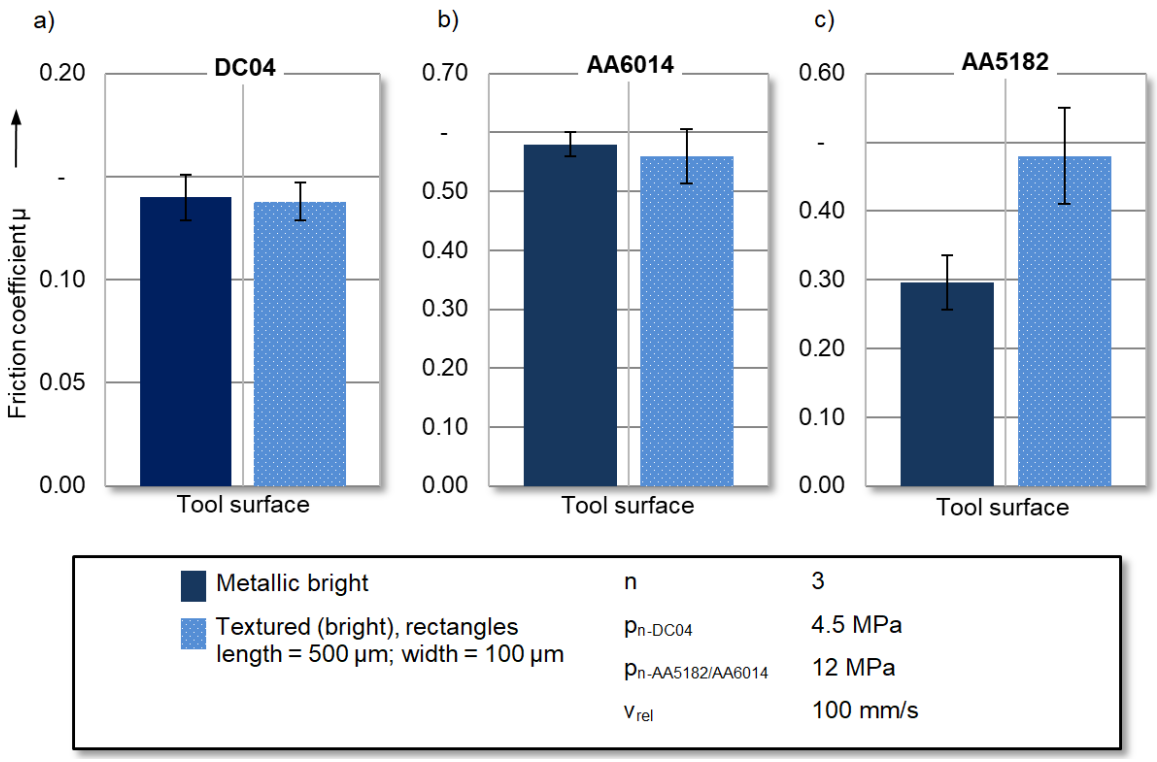

Fig. 17: Friction coefficient measured in strip drawing tests under dry condition for a metallic bright and a metallic bright textured surface; a) in contact with DC04; b) in contact with AA6014; c) in contact with AA5182 [41]

For strip drawing tests with aluminum, the alloys AA6014 and AA5182 are investigated. Tests with AA6014 showed that the metallic bright surface shows a maximum friction above 0.57 which would indicate local plastic deformation of sheet material according to the von Mises yield criterion. The friction coefficients for the metallic bright textured tool surface vary between 0.5 and 0.6. Thus, no significant decrease can be measured. For the AA5182 the strip drawing test shows an increased friction with $\mu = 0.49$ for the metallic bright textured surface compared to the metallic bright surface ($\mu = 0.3$). These strip drawing tests indicate a high influence of the sheet material if a direct tool/workpiece contact is present. In tests with DC04 a low adhesion tendency of zinc against tool steel causes low friction. In contrast, the aluminum alloy AA5182 shows higher adhesion tendency towards steel in dry deep drawing leading to high friction coefficients [41]. In a second step, the resulting friction jaw surfaces are characterized using confocal microscopy. For DC04 the metallic bright jaws show no visible signs of wear while the textured jaw showed a small amount of zinc adhesion in the region of the structure edges (see Fig. 18) [41].

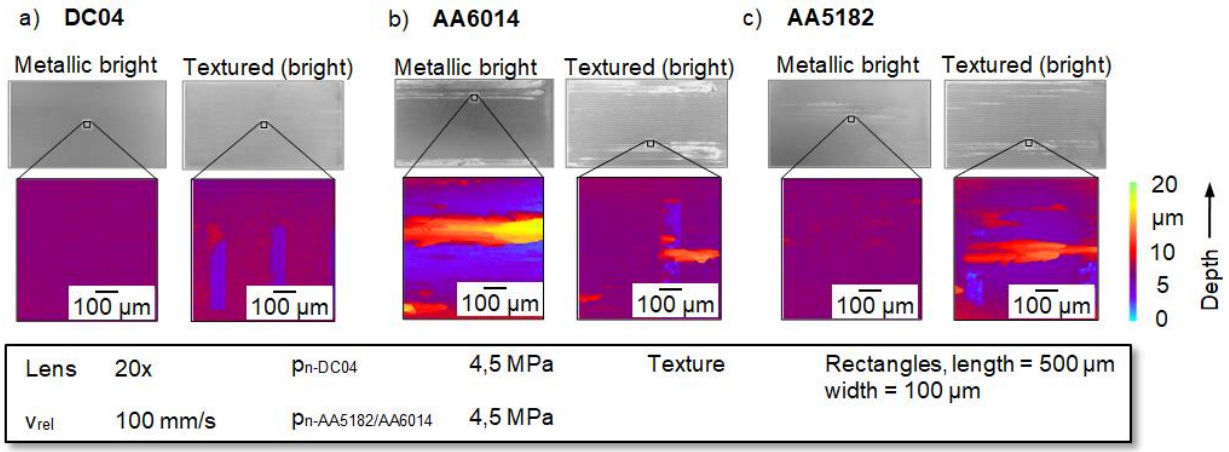

Fig. 18: Friction jaw surface after strip drawing tests; a) with DC04; left) metallic bright surface; right) metallic bright textured surface; b) with AA5182; left) metallic bright surface; right) metallic bright textured surface; c) with AA6014; left) metallic bright surface; right) metallic bright textured surface [41]

For both aluminum alloys, strong adhesion occurred in strip drawing tests with metallic bright as well as with textured surfaces (see Fig. 18 b) and c)) [41]. The results of the optical characterization of the surfaces are in good coincidence with the friction coefficients resulting from the strip drawing tests. For the textured as well as the non-textured surface, the main reason for the increased amount of wear is the strong adhesion tendency of the aluminum alloys. These results show that the tested surface textures as a standalone modification are not suitable to improve the tribological conditions in dry deep drawing due to the increased adhesion tendency. Therefore, a combination of surface coating and texturing was investigated.

5.2 Ultrafast pulsed laser finishing of a-C:H coatings

As previous studies have shown, a-C:H coatings are a possibility to improve the tribological conditions in dry deep drawing. However, the roughness of the tool surfaces has a major effect on the tribological conditions in deep drawing under dry conditions [42]. Since the coating process itself leads to an increased amount and height of roughness asperities, the surface needs to be post-treated. Especially for complex geometries, this is conventionally done by manual polishing. In the course of the project, an ultrafast pulsed laser finishing technique was investigated as an alternative to mechanical post treatment. Here, a laser based technique offers the benefits of contactless and - due to high speed deflection - fast machining which additionally offers the possibility of easy automation.

Therefore, a laser based smoothing approach of a-C:H coated surfaces was analyzed with regards to its ability to reduce the surface roughness. Furthermore, the resulting friction and wear for these treated surfaces were analyzed in strip drawing tests. The friction jaws were made of 1.2379 with a substrate hardness of about HRC 60 ± 1 and coated with a-C:H as described in chapter 4.1.2 as well as in [43].

In ultrafast laser finishing, a Gaussian beam is scanned across the coated surface. Here, a mode-locked Nd:YVO_4 laser (Fuego, Time-Bandwidth Products) operating at a wavelength $\lambda = 1064$ nm and a pulse duration $\tau_p = 10$ ps (FWHM) was used. A f-theta lens with a focal length $f = 160$ mm was used to create a diameter at the beam waist ($1/e^2$) of $d_0 = 30$ µm. The focused laser beam was deflected by a galvanometer scanner (hurryScan 14 II, Scanlab AG). The selection of the used process parameters as well as an analytic model describing the resulting surface geometry is explained in detail in [43]. The laser finishing approach is evaluated regarding the reduced peak height S_{pk} as shown in Fig. 19.

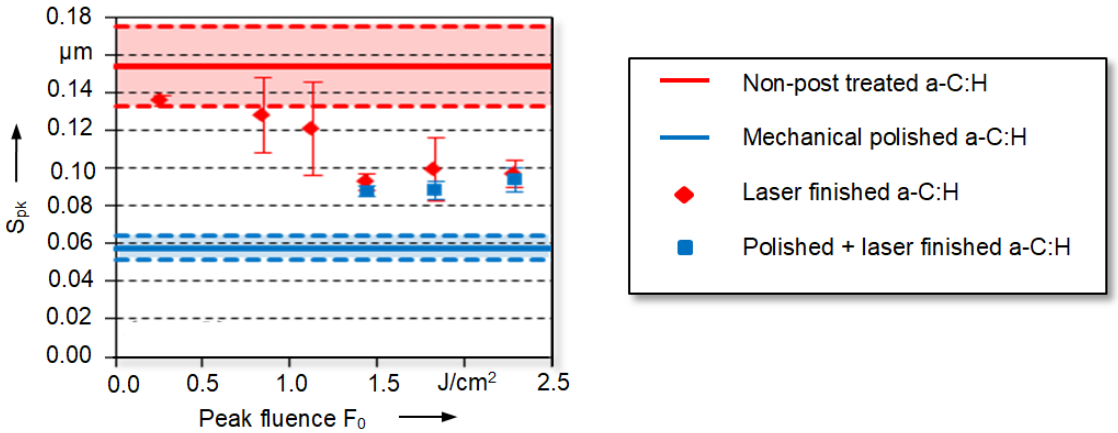

Fig. 19: Reduced peak height vs. used peak fluence in laser finishing for a laser finished a-C:H surface (red diamond) as well as a polished and afterwards laser finished a-C:H surface (blue square). As a reference, a non-post treated a-C:H surface (red line) and a polished a-C:H surface is shown. [43]

Here, four different surface treatments are compared. A non-post-treated, coated surface indicates the initial surface roughness before the laser finishing process. As a reference, a mechanically post-treated surface is shown and compared to the surfaces resulting from either the laser finishing process or a combination of mechanical post-treatment followed by laser finishing. For peak fluences below 1.0 J/cm² the roughness of the laser finished surface is in the range of the non-post-treated surface. For higher peak fluences the roughness is significantly decreased. A minimal surface roughness is achieved by laser finishing with 1.5 J/cm² [43]. At this fluence, the roughness of the resulting surface is in the same range as for a combination of mechanical and laser finishing. However, the resulting reduced peak height for laser

finishing is still larger than for mechanical polishing. The mechanism of the surface smoothing is the ablation of the roughness asperities resulting from the coating process. For sufficient pulse energies these asperities are ablated by scanning across the surface. At the position of the roughness asperities craters remain, which lead to improved tribological conditions. The topography of the surface resulting from laser finishing is compared to the initial surface in Fig. 20. For laser finishing, a fluence of 1.5 J/cm^2 is used. Here, the surface roughness is mainly reduced due to the removal of asperities by laser ablation.

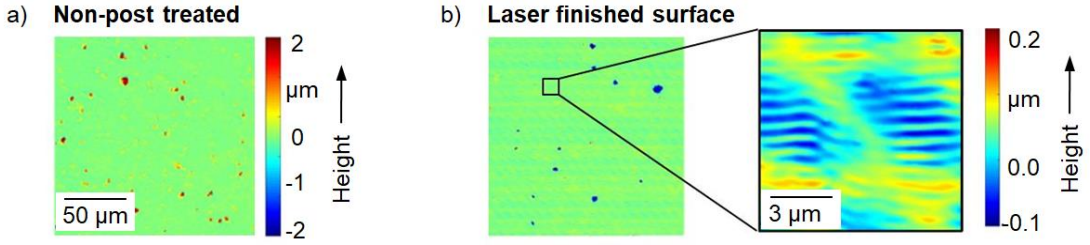

Fig. 20: Laser scanning microscopy of a-C:H coated surfaces; a) directly after the coating process; b) laser finished surface [43]

To evaluate the use of laser finished surfaces in dry deep drawing, strip drawing tests were carried out against DC04 and AA5182 (see Fig. 21). [43]

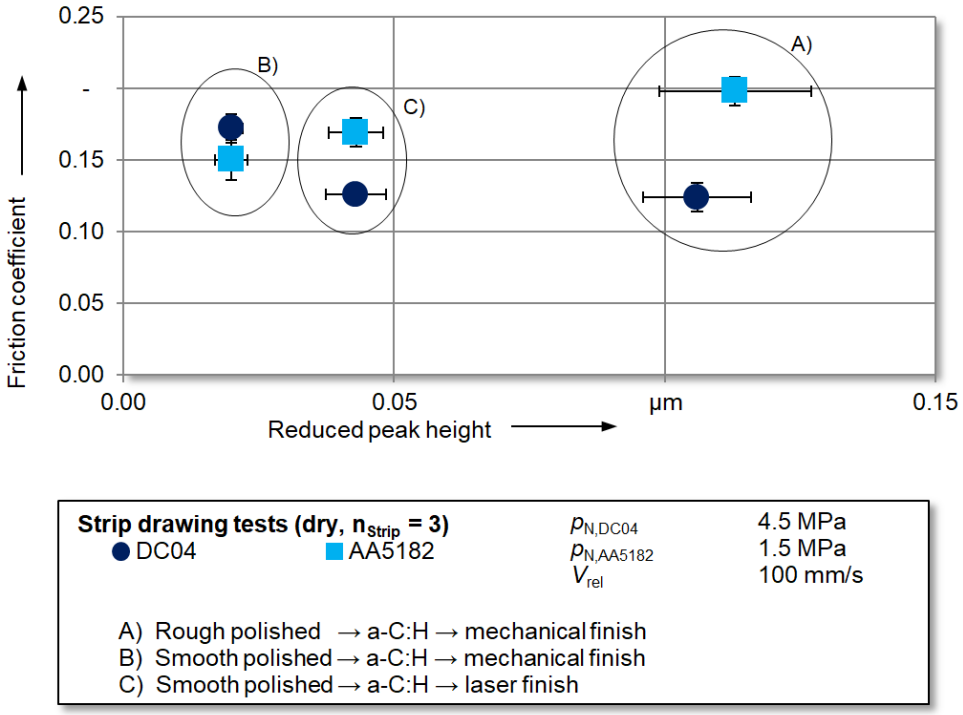

Figure 21: Dry deep drawing tests with different post treatment approaches of a a-C:H coating [43]

For comparison, friction jaws with different surface post-treatments are shown. (A) shows a rough polished, coated, mechanically finished and (B) a smooth polished, coated, mechanically finished surface. In (C), the friction jaws were smooth polished, coated and afterwards laser finished with laser parameters resulting in the lowest reduced peak height as described in [43].

With smooth polished friction jaws, similar friction coefficients for DC04 and AA5182 were measured. With increasing tool roughness, both materials show a different behavior. For DC04 the friction slightly decreases. In contrast, the friction for AA5182 increases with increasing roughness. After the strip drawing test the surface was evaluated in terms of wear. For (A) and (C) strong adhesion was visible while variant B only showed minimal adhesion.

5.3 Pico-second laser based surface modification of ta-C coated surfaces

As shown before, diamond-like carbon (DLC) coatings can be used to substitute the lubricants in dry deep drawing. To adapt the tribological conditions locally, and therefore enable the steering of the material flow in deep drawing, surface adaption on a macroscopic scale by laser ablation is one possibility [44]. For the described investigations, surface texturing of a tetrahedral amorphous carbon (ta-C) coating with a thickness of 0.6 µm is chosen, since this coating type led to low wear and friction in tribological tests [45]. Picosecond laser based texturing is chosen since it enables surface texturing with minimal heat affected zones (HAZ). Therefore, the surface topography can be influenced without changing the chemical properties of the heat sensitive coating. By applying well-chosen processing parameters material ablation with minimal HAZ as well as local heat treatment by heat accumulation can be realized [45].

5.3.1 Texturing of ta-C coatings with a wavelength of 1064 nm and 355 nm

Different texturing strategies were evaluated in terms of the resulting surface properties and their relative structuring efficiency. These different strategies enable either the local ablation of the complete coating thickness or local texturing of the coating with a defined depth smaller than the coating thickness enabling a closed structure bottom without metallic surfaces. For the first texturing approach a picosecond laser (described in 5.2) with pulse duration $\tau_p = 10$ ps and a wavelength of 1064 nm was used [45]. A Gaussian beam with a beam diameter of about 30 µm was scanned across the surface. Since the ta-C coating is highly transparent for this wavelength no ablation based on linear absorption is possible. Therefore, another ablation mechanism is tested. Here, the light is transmitted through the coating and absorbed in the underlying chromium layer. The chromium layer is heated which induces strong pressure growth in the interface between both layers. In regions where this pressure exceeds the shear strength of the ta-C coating this top layer is removed [45]. An exemplary surface texturing result for this approach is given in Fig. 22 [45]. The described ablation mechanism is indicated by the remaining flake on the right side of the crater. Moreover, the exposed metallic structure bottom as well as the line shaped structure (Fig. 22 b)) indicates the spalling of the whole ta-C layer. [45].

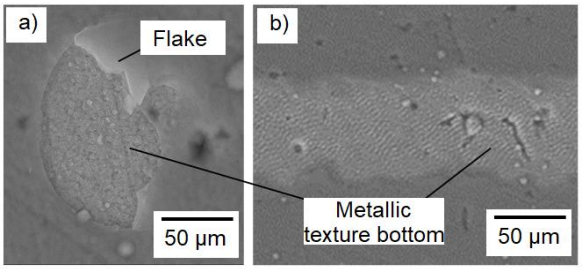

Fig. 22: Edges of a) crater and b) line-shaped structures generated by ablation with λ = 1064 nm (f_P = 1 kHz, $w_0 \approx$ 15 µm, F = 0.31 J/cm², No. of scans S = 1; p_x = 4 µm)

Since this mechanism leads to a limited freedom of shape a second texturing approach is tested. Here, a wavelength of 355 nm was used. The beam diameter was kept constant at 31 µm [45]. At 355 nm, the absorption in the coating allows direct texturing with a defined depth and thus a structure bottom which shows a remaining ta-C coating.

Therefore, ultrafast laser based processing of a ta-C layer can be performed with different ablation mechanism corresponding to different laser wavelengths. An infrared wavelength which is transmitted through the coating can be used for surface texturing when the whole thickness of the ta-C layer should be removed. Alternatively, ultraviolet laser radiation can be used, where advantage can be taken of an increased freedom of texture form and the possibility of a defined local chemical change of the coating. Texturing parameters used in the following experiments for both ablation techniques are given in Tab. 8.

Tab. 8: Laser processing parameters for micro texturing

Set	Wavelength λ (nm)	Fluence F (J/cm²)	Pitch distance p_x (µm)	Hatch distance p_y (µm)	No. of scans S
A.1	1064	0.3	7	10	1
A.2	1064	1.3	2	10	5
B	355	0.6	5	8	2

For the tribological characterization, six different geometries were generated and evaluated in strip drawing tests. The rectangular geometries (R20d, R35d, R50d) with a length of 500 µm and a width of 200 µm differ by their degree of coverage (20 %, 35 %, 50 %). The depth of these textures is 6 µm. They are generated by first applying the parameter set A.1 (Tab. 8) to locally remove the ta-C coating. In a second step, the parameter set A.2 is applied to ablate the steel substrate and increase the depth of the texturing. The increased volume can work as a reservoir removing wear particles from the contact zone. Moreover, the rectangular texturing (R35f) and a line-shaped texture (L35f) are generated by only applying A.1 to remove the ta-C coating. As an additional texture variant the line shaped texture (L35f*) is generated by applying the parameter set B.

After the laser based texturing, the friction jaws are cleaned in an ultrasonic bath with isopropyl alcohol to remove possible particles originating from the laser process. The strip drawing tests are explained in detail in chapter 3. Additionally, the sample surface was characterized before and after laser processing as well as after strip drawing tests topographically with a laser scanning microscope. Moreover, the chemical properties of the modified ta-C layers were analyzed by Raman microscopy with an excitation wavelength of 532 nm (alpha 300RA, WITec) which is described in detail in [45]. For processing of a ta-C an ultrafast laser can be used in different regimes. On the one hand, an infrared wavelength which is transmitted through the coating can be used. The ablation mechanism is here the spalling off of the whole ta-C layer due to the expansion of the underlying chromium layer. Alternatively, with the benefit of an increased freedom of texture form and the possibility of a chemical change of the coating, ultraviolet laser radiation can be used. Here, the laser is linearly absorbed within the layer. Therefore, a large variety of textures, i. e. with closed ta-C bottom, can be created.

5.3.2 Experimental results of ultrafast laser based texturing with 1064 nm and 355 nm

For the experimental realization of ultrafast laser texturing a wavelength of 1064 nm was used to create the textures with the edge shape geometry shown in Fig. 23 a). Here, a pulse overlap towards the scanning direction of 78 % already leads to a variation of the width of the textures by only $\pm$ 1.15 µm corresponding to 0.6 % of the structure width. As expected, the structure bottom shows an uncovered chromium layer.

As a comparison, texturing with 355 nm gives the possibility to continuously adjust the feature depth and thus enables a closed ta-C layer. Moreover, the chamfer angle β can be controlled using this structuring approach (Fig. 23 b)). The shape of the structure edge is shown in Fig. 23. The width varied by about 0.38 µm corresponding to 0.02 % indicating a precise texturing. Even though the additional degrees of freedom in the geometry of the generated textures offer more possibilities for influencing the tribological behavior, induced heat by the ablation process will lead to a chemical modification of the ta-C layer. To be able to estimate the thermally induced sp^2 hybridization from the ablation process, and thus predict suitable process parameters leading to a low degree of sp^2 hybridization, numerical simulations were performed. To this end, a solid heat transfer model in COMSOL (Comsol Multiphysics) was extended for ps laser modification at a wavelength of 355 nm of a ta-C coating [46]. Results with these predicted parameters are shown in Fig. 23 e). Here, still a significant increase of the sp^2 phase in a 2 µm broad region results from the excess energy input and the residual heat.

The results in Fig. 23 show the benefits and drawbacks of each tested texturing approach. Thus, depending on the requirement of the desired texture, the appropriate texturing approach has to be selected. If structuring with a closed ta-C structure bottom or a defined chamfer angle is required, 355 nm has to be applied. With this approach also the chemical composition of the coating can be changed. Otherwise, a wavelength of 1064 nm can be used for a fast and efficient ablation of the whole ta-C layer with a single pulse.

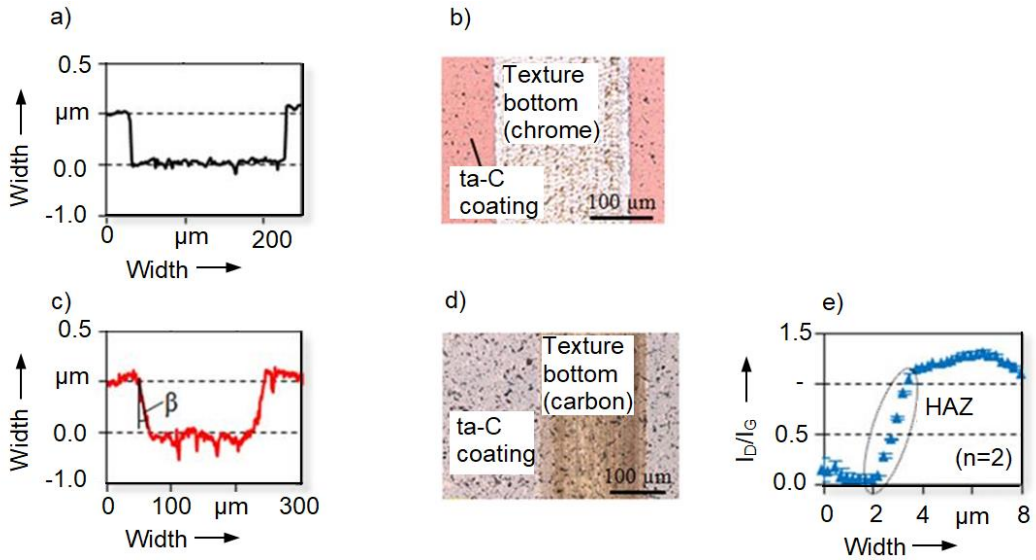

Fig. 23: Cross section (a, c), top view (b, d) and I_D/I_G-ratio at the edge (e) of structures generated with 1064 (parameter set A.1 see Tab. 8) and 355 nm (parameter set B see Tab. 8), respectively

5.3.3 Tribological behavior of textured ta-C coatings

As mentioned before, micro textures are one approach to adjust the tribological conditions. Therefore, the effect of the generated textures is analyzed in strip drawing tests with DC04 and AA5182. For DC04 only the rectangular texture variants with metallic structure bottom are tested. These tests showed that the variant R20d with a degree of coverage of 20 % as well as R35d with a degree of coverage of 35 % led to a reduction of the friction coefficient due to the reduced effective contact area as shown in Fig. 24 [45].

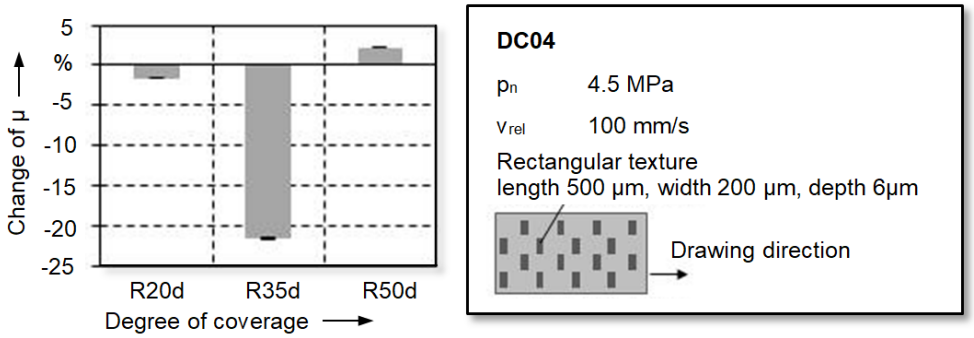

Fig. 24: a) Changes of friction coefficient μ due to microstructures in ta-C coated tool surfaces in contact with DC04 [45

Here, the increased contact pressure induces smoothing of the sheet surface leading to a reduced amount of roughness asperities and therefore, a reduced friction coefficient. If the degree of coverage is increased to 50 % (R50d) the friction increases. This increase might be caused by a larger amount of asperities which are shared at the edges of the texturing which negates the positive effect of the reduced effective contact area [45].

For strip drawing tests with AA5182 first the texture variant R35d which led to the lowest friction against DC04 was tested. In this case, the friction was increased to 200 % of the non-textured reference. This increase occurred due to the adhesion of aluminum at the edges of the texture perpendicular to the drawing direction [48]. Therefore, different texturing variants with different shapes were evaluated. For the texture variant R35f the same friction coefficient as for the deep texture was measured (Fig. 25). To get rid of adhesion on structure edges perpendicular to the drawing direction, a line shaped texturing was tested. This texture variant had a depth of 0.6 µm and a degree of coverage of 35 %. The resulting friction coefficient was 215 % above the non-textured reference (Fig. 25). Meaning that, even though, the interaction of asperities and edges perpendicular to the drawing direction is prevented by the line shaped geometry the friction increases.

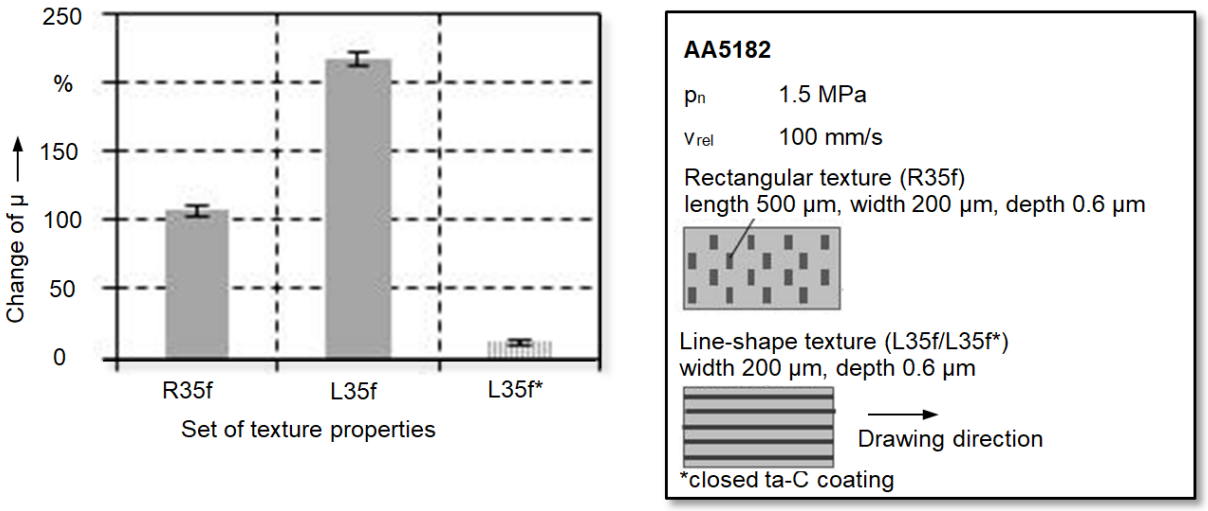

Fig. 25: Changes of friction coefficient μ due to 0.6 µm deep microstructures in ta-C coated tool surfaces in contact with AA5182 [45]

The increase of the friction coefficient might be explained by the interaction of asperities of the sheet surfaces which are in the region of the line-shaped areas and therefore in contact with the metallic structure bottom [48]. Due to the strong adhesion tendency of aluminum, the dry contact with a non-coated surface could explain the increased friction. To prevent any contact between the sheet material and the metallic substrate surface, a thicker ta-C coating is generated and prepared with a line-shaped texturing (L35f*) having a depth of 0.6 µm and therefore a closed ta-C layer. This texture variant is generated with a wavelength of 355 nm and the parameter set B (Tab. 8). Strip drawing tests with this surface variant showed a friction coefficient which was 10 % higher than the non-textured reference. The reason for this increase might be the thermally induced sp^2 hybridization at the texture bottom. The increased sp^2 content leads to a reduced coating hardness and therefore results in slightly higher adhesion tendency for AA5182. These tribological investigations show that direct contact of aluminum sheet material with the non-coated substrate surface needs to be avoided and that structuring with a wavelength of 355 nm can be used to this end.

5.4 Texturing of cylindrical surfaces

In addition to flat surfaces, real tool geometries require the processing of curved geometries. Therefore, cylindrical surfaces were structured with a setup similar to the texturing setup described in chapter 5.2 but extended with a linear x,y,z-stage system and a rotation stage enabling the rotation around the cylinder axis. The workpiece surface was placed in the focus of the f-theta-lens. An ultrafast laser beam with Gaussian intensity distribution was scanned across the surface to locally ablate the coating material. Caused by an imperfect alignment of the workpiece axis with the axis of the rotation stage, the surface position varies while rotating the workpiece. To minimize the change of height as well as the change of the lateral position during the rotation the linear stage system is synchronized to the rotation and compensates the positioning errors. Therefore, the coincidence of focal plane and workpiece surface was ensured. Using this setup metallic bright cylinders as well as ta-C coated cylinders were textured. As geometry rectangles with a length of 200 µm, a width of 500 µm, a depth of 5 µm, and a degree of coverage of 35 % are chosen, since these show the lowest friction coefficient in flat strip drawing tests. These surface textures were evaluated by means of their tribological conditions in dry deep drawing in bending rotation tests against DC04 and AA5182. These tests are described in chapter 3.1 and model the flange area in deep drawing. The friction coefficients measured in bending rotation tests are shown in Fig. 26 a) for DC04 and b for AA5182. For DC04 the friction coefficient for each textured sample is in the same range as the non-textured sample. Unlike the flat strip drawing tests the friction coefficient could not be significantly reduced. This might be explained by the higher contact pressure of 22 MPa and therefore an increased interaction of roughness asperities at the structure edges. This contact pressure is a realistic value for the pressure in the flange area in dry deep drawing. For AA5182 the friction coefficient of the textured samples is increased in comparison with the non-textured samples. This behavior verifies the results of the before mentioned flat strip drawing test.

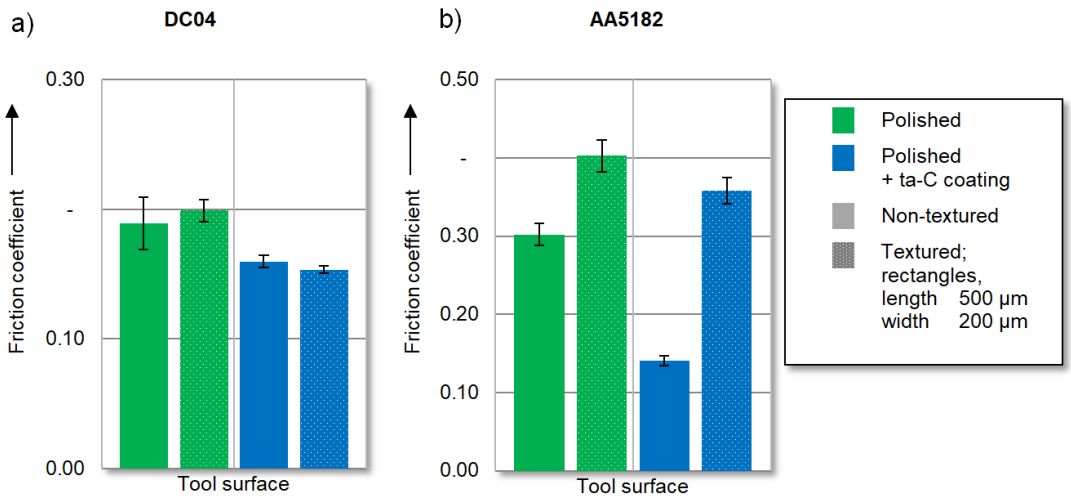

Fig. 26: Bending rotation tests of textured and non-textured cylindrical surfaces with and without ta-C coating

5.5 Beam profile shaping for efficient structuring

To increase the efficiency of ultrafast laser based surface modification and therefore enable the economic use of these textures in dry deep drawing on a large scale beam profile shaping is evaluated. In ultrafast laser processing using a Gaussian intensity distribution, the most efficient peak fluence for material ablation is given as $F_{0,max} = e^2 F_{th}$ with F_{th} being the ablation threshold of the material. Nowadays, high power ultrafast laser sources are already available and the development to increasing pulse energies and pulse repetition rates is still ongoing. Unfortunately, using high pulse energies and fast repetition rates for efficient material removal is not trivial, since an increased pulse repetition rate requires an increased beam deflection speed to prevent heat accumulation. On the other hand, increased pulse energy leads to decreased ablation efficiency. Beam shaping is one possibility to overcome these problems by distributing the energy of a pulse over a large area with a predefined shape.

In the project, a phase-only liquid crystal on silicon spatial light modulator (LCOS- SLM) was used to evaluate different beam shaping techniques. All investigated techniques realize beam shaping by a phase change in the Fourier domain. Therefore, a locally varying phase retardation (also called phase mask) is applied at the LCOS-SLM which allows controlling the intensity distribution in the image plane. To calculate the required phase retardation, the Gerchberg-Saxton (GS) algorithm can be used [47]. However, to fully control the light field, the control of amplitude and phase are necessary. Since the LCOS-SLM does only influence the phase in the Fourier plane while the amplitude of the incident beam is unchanged the degrees of freedom are limited. Due to the limited degrees of freedom the algorithm does not allow to control the phase distribution in the image plane leading to a randomly distributed phase. Therefore, constructive and destructive interference of the light which is diffracted towards the designed beam profile causes the formation of speckle. For beam shaping using the GS algorithm, an exemplary focal intensity distribution is given in Fig. 27 [47]. As a target intensity distribution a rectangular flat-top was used (see Fig. 27 a)). An experimental read-out for a single phase mask shows pronounced speckle as shown in Fig. 27 b). If such an intensity distribution is used for texturing, the ablated geometry will differ from the target geometry. Therefore, different speckle reduction techniques are investigated. The first technique is averaging of speckle patterns, where different phase masks for the same target distribution but with statistically independent speckle patterns are calculated. If the read-out of these phase masks are averaged, the intensity distributions shown in Fig. 27 c) for 36 phase masks and Fig. 27 d) for 64 phase masks [47]. Averaging more than 64 phase masks does not further improve the homogeneity of the intensity profile.[48]

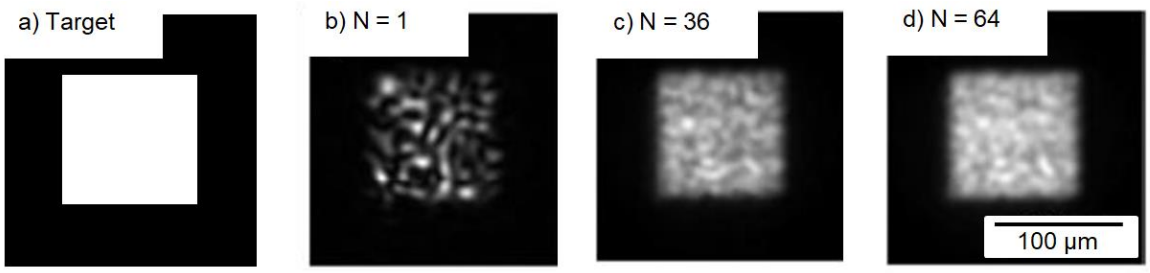

Fig. 27: Speckle distribution from LCOS-SLM beam shaping; a) target intensity distribution; b) read-out of a single phase mask; c) average of the read-outs of 36 phase masks for the same target beam shape; d) Average of the read-outs of 64 phase masks for the same target beam shape [47]

Averaging different read-outs, however, is only feasible for processes where many pulses, at least enough for good averaging, are needed for generating the desired feature. In addition, relatively slow switching times of LCOS-SLMs limit the speed at which different phase masks can be applied and therefore this approach is only practical if a very low repetition frequency of the laser is used anyway. For the SLM used in the experiment the manufacturer states a switching rate of 60 Hz. If no laser pulses are applied during the switching time, the overall process efficiency is reduced. Therefore, alternative techniques were evaluated, where the switching rate of the SLM is not the limiting factor.

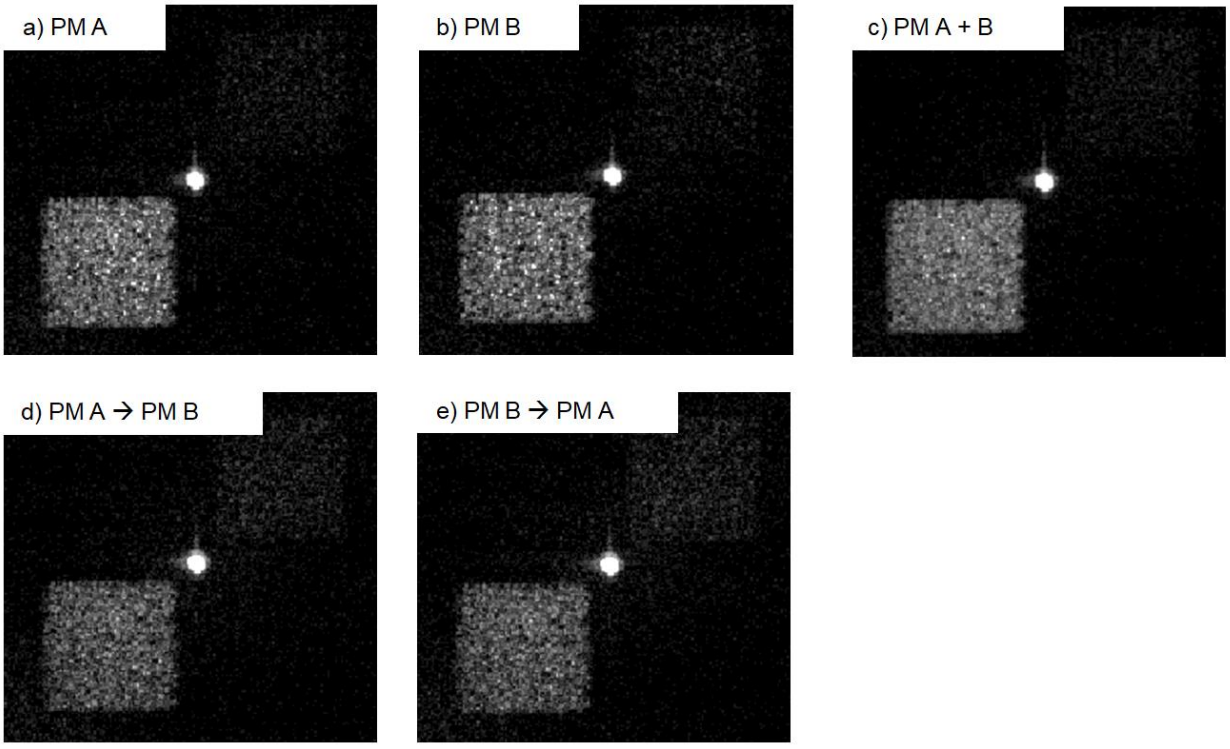

Fig. 28: Speckle distribution from LCOS-SLM beam shaping; a), b): with unchaining phase mask A or B; c): averaged read-out of phase masks A + B; d), e): read-out during switching time of the LCOS-SLM

One of these approaches actively uses the switching time for averaging. During changing from one phase mask to another, at each LCOS-SLM pixel birefringent crystals are rotated. Therefore, a gradual change from one phase mask to the other takes place. To evaluate if the switching time can be used for structuring and how efficiency and beam quality are influenced, high speed video recordings are taken with a framerate of 100 kHz. In the experiment two different phase masks calculated with the GS algorithm are applied. As a laser source a cw-laser at wavelength of 633 nm was used. Fig. 28 shows the read-out for both masks as well as a superposition of both read-outs and the read-out during the switching of the LCOS-SLM. For mask A and B speckles are strongly pronounced and the distribution differs from each other (Fig. 28 a) and b)). The average of both read-outs as well as the read-outs during the switching processes show a more homogenous beam profile (Fig. 28 c), d), and e)).

To evaluate the beam quality the speckle contrast $C = \frac{\sigma_I}{I_{mean}}$ is chosen [49]. It represents the normalized standard deviation within the target intensity divided by the mean intensity. For a homogenous beam profile C is close to zero. For the evaluation of the relative diffraction efficiencies during the switching process the pixel sum within the target intensity region is summed and divided by the highest efficiency which is reached when the switching process is finished. In Fig. 29 the speckle contrast as well as the relative diffraction efficiency is shown. Although the efficiency is reduced by up to 50 % the Speckle contrast is reduced by 5 % down to 0.76.

The second approach is the double constraint Gerchberg-Saxton (DCGS) algorithm, described in detail in [47]. In the DCGS no averaging is done to improve the homogeneity enabling single shot beam shaping. Here, regions of the Fourier plane that would lead to destructive interference in the image plane are diffracted away from the targeted intensity distribution. By doing so, the phase in the image plane can be controlled leading to a reduction of speckle. However, this additional degree of freedom corresponding to amplitude and phase modulation in the Fourier plane goes along with a loss of efficiency.

A read-out for the DCGS is shown in Fig. 29 b) [47]. Here, the diffraction efficiency was reduced by about 80 %, while the speckle contrast could also be reduced by about 80 %. Although the diffraction efficiency is relatively low, the gain of homogeneity will be advantageous for precious ablation.

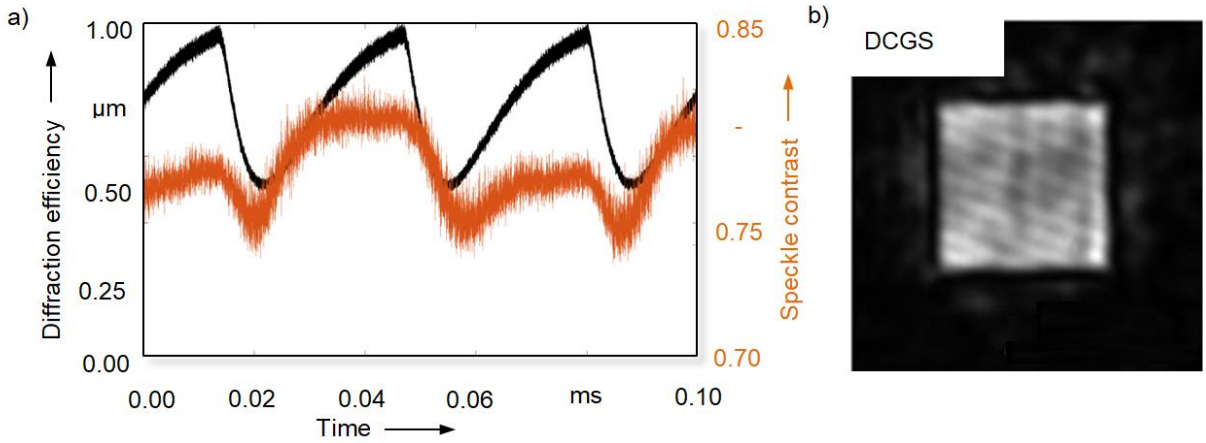

Fig. 29: a) Efficiency and speckle contrast during the switching time of a LCOS-SLM., two different phase masks with the same target intensity are applied. b) Read out of double constraint Gerchberg-Saxton (DCGS) algorithm.

6 Evaluation of measures for dry deep drawing in forming processes

Laboratory tests have shown that measures such as the coating systems a-C:H and ta-C are suitable to meet the challenges of dry deep drawing and reduce friction as well as wear. For a full evaluation of these modifications they are applied in forming processes. In addition, their long-term application behavior was analyzed.

6.1 Experimental analysis of forming processes

The first part of the evaluation of the measures was conducted in single stroke forming processes. For this purpose, the process for forming rectangular cups presented in [15] and section 3.3 was used for the workpiece materials DC04 and AA6014. In this process the blankholder and the die were modified by coating systems. For both workpiece materials, the lowest forming force is achieved with lubricated workpieces, due to lowest friction. The analysis of the force-displacement curves for DC04, shown in Fig. 30 a), indicates a comparable shape for uncoated tools as well as coated and post-polished tools, because no wear and thus only a slight increase in friction occurred in laboratory tests for the limited number of forming operations. The usage of a ta-C coated and not post-polished tools – which have a higher roughness than the uncoated tools – causes the highest forming force. This confirms the results of the laboratory tests and highlights the necessity of a post-treatment of the coatings. In the case of AA6014, see Fig. 30 b), the use of uncoated tools or coated but not post-polished tools leads to failure of the component before reaching the maximum drawing depth due to excessive friction. This confirms the findings of laboratory tests that dry deep drawing of AA6014 is more critical than DC04 due to higher friction. By using the coated and post-

polished tools, dry deep drawing of AA6014 components is possible without component failure. Thus, dry deep drawing processes can be realized by using post-polished ta-C and a-C:H coatings. In [20] dry deep drawing tests with AA5182 are shown. These indicate a similar behavior as AA6014.

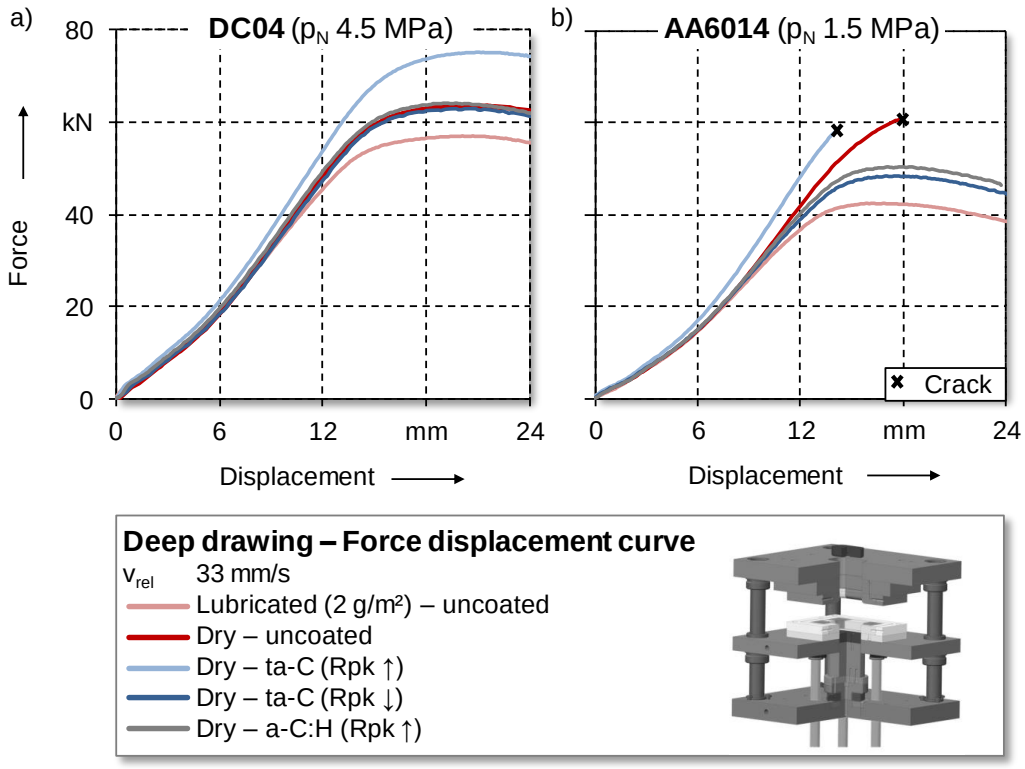

Fig. 30: Force displacement curves for deep drawing with differently modified tools for a) DC04 and b) AA6014 in accordance to [20]

In order to use the advantages of forming technology with regard to efficient production of large quantities of high-quality components, a long tool life and thus also high durability of measures are necessary. To evaluate tool wear, the roughness of the coatings before and after the forming of ten cups of the wear-critical workpiece material AA6014 is analyzed in Fig. 31. No increase in roughness or wear can be determined for either the coating system ta-C or a-C:H. Thus, the measures prevent adhesion. The forming of ten components is, however, not sufficient to fully evaluate the durability of the measures. This motivates the development of a novel wear test rig to investigate the application behavior of the coatings for a high number of forming operations presented in section 6.2.

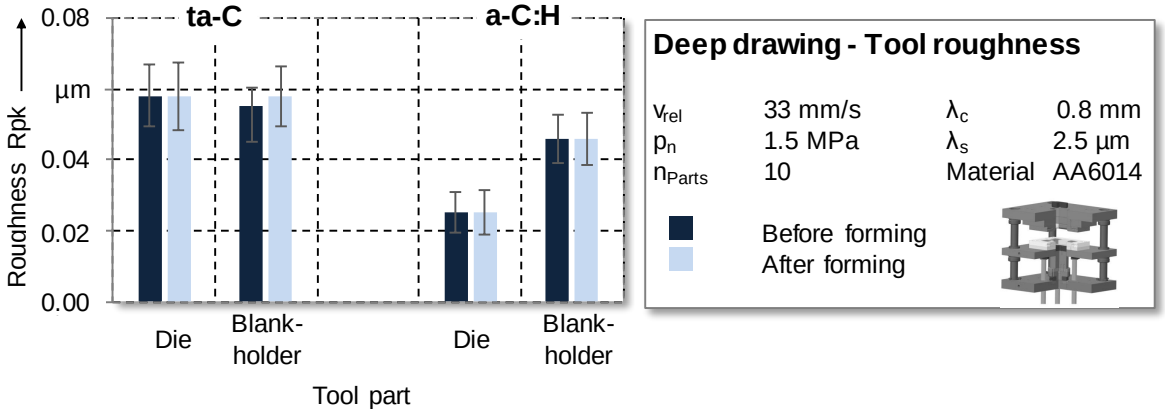

Fig. 31: Tool roughness for modified tool before and after forming in accordance to [20]

6.2 Experimental analysis of wear

As described in section 6.1, a large number of forming operations is required to fully evaluate the durability of the measures. In a single stroke process this is not feasible. Consequently, a new test rig was developed within the scope of the research project producing a large number of components within a reasonable period of time. For this purpose, a forming process with a process chain consisting of automated material feed and a progressive die for dry deep drawing of cups was designed, see Fig. 32 a). By integrating the tooling system on a high-speed press, 100 components per minute can be automatically produced. The progressive die consists of four stages as illustrated in Fig. 32 b). In the third stage, a round blank with an outer diameter of 62.0 mm is deep drawn into a flangeless cup with an outer diameter of 42.8 mm. The design of the tool geometry as shown in in Fig. 32 c) and the process kinematics of the tool system are described in detail in [50]. The test rig was utilized to investigate the durability of the post-polished a-C:H and ta-C coatings, which were identified as suitable in the laboratory and single stroke tests, for the workpiece materials DC04 and AA5182. 3 000 parts were produced with all modifications. Uncoated tools were analyzed as references. For DC04 and AA5182 the tests with uncoated tools were stopped after the forming of 200 respectively 10 cups due to excessive wear.

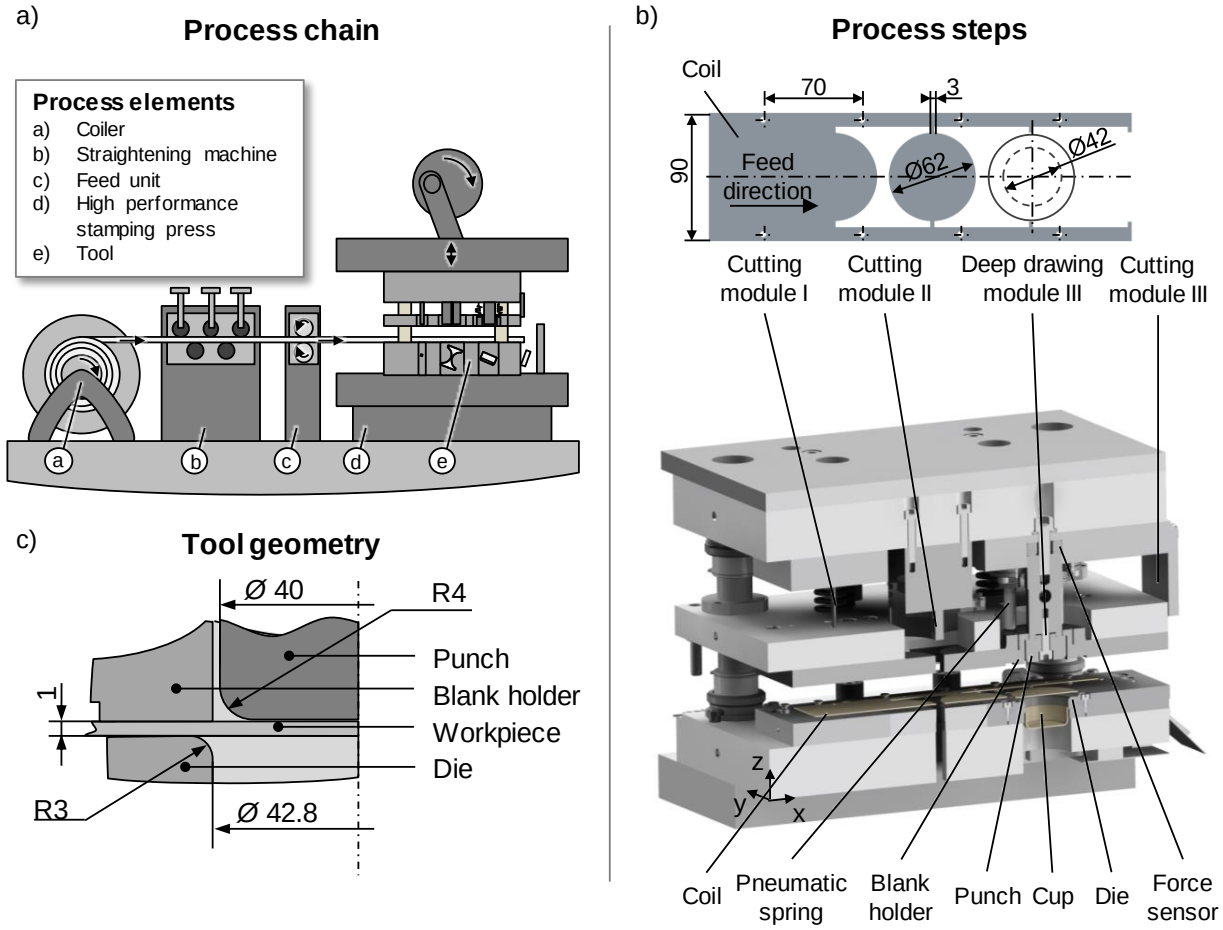

Fig. 32: Novel test rig for the investigation of the wear of measures for a high quantity of parts: a) process chain, b) process steps and c) tool geometry

The analysis of the die topographies after forming (Fig. 33) reveals a wear behavior specific to the workpiece material and tool surface. For the uncoated tools, significant wear was identified on the radius of the die after 200 strokes with DC04 and after 10 strokes with AA5182. The local wear at the radius is due to the highest tribological stresses in this area [16]. It was identified in [50] by EDX-measurements as adhesion. The roughness for uncoated tools indicates that the reduced peak height R_{pk} increases from 0.05 µm to values between 2.00 µm and 3.00 µm after only 5 forming operations and then remains at this level. When applying the a-C:H and ta-C coating for the production of components made of DC04, no change in the topography can be detected. The roughness tends to decrease due to shearing of droplets. Even with the ta-C coating in combination with the more wear-critical AA5182, the roughness decreases slightly due to this effect and no

adhesion occurs. When forming AA5182 with a-C:H coated tools, however, minor adhesion to the drawing ring radius occurs after 3 000 cups. This is confirmed by roughness measurements, in which the roughness increases after 1 000 strokes. Thus, it was shown that the measures investigated are suitable to completely prevent or significantly reduce wear for a high number of forming operations. This verifies the findings of the laboratory tests.

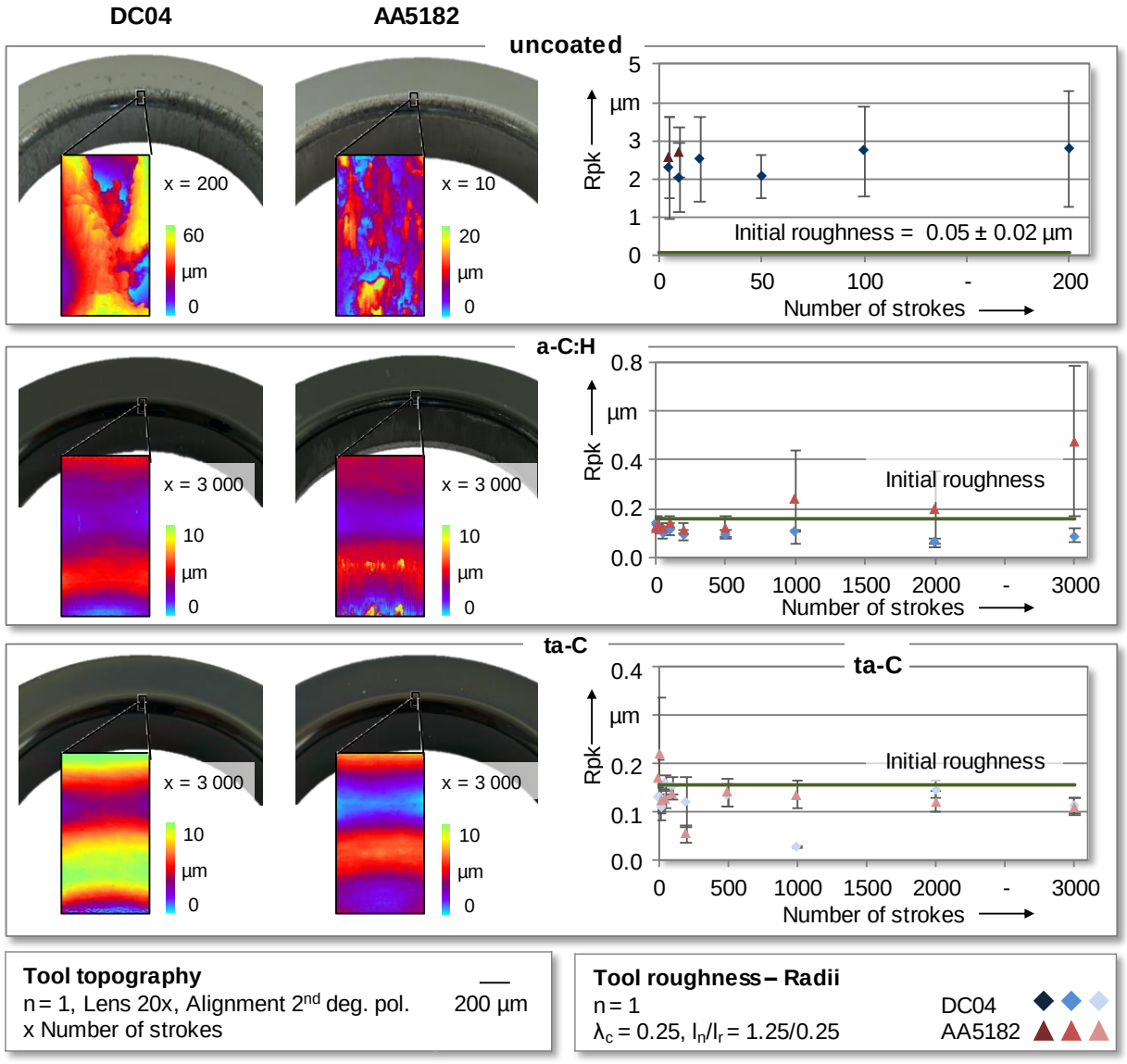

Fig. 33: Analysis of tool wear for high number of dry deep drawing operations

In addition to the tool topography, the surface of the components is of particular importance, since this influences, for example, the paintability [51]. The quality of the component surface is influenced by the condition of the tools and thus by wear. To determine the relationship between wear and component quality, the components were analyzed. Fig. 34 shows the topographies of the components at the end of the tests. For all components a change of the surface in comparison to the original texture occurs in the area of the frame. This is caused by the relative movement of the workpieces to the drawing ring. For cups that were formed with non-modified tools, the surface roughens strongly due to the adhesive wear of the tools. Grooves were also apparent on cups made of AA5182 that have been formed with a-C:H coated tools due to wear of these tools, see Fig. 32. No grooves occur on all other surfaces. The coating systems are therefore suitable for improving the component quality. A detailed analysis of the roughness of the workpiece surface is discussed in [50].

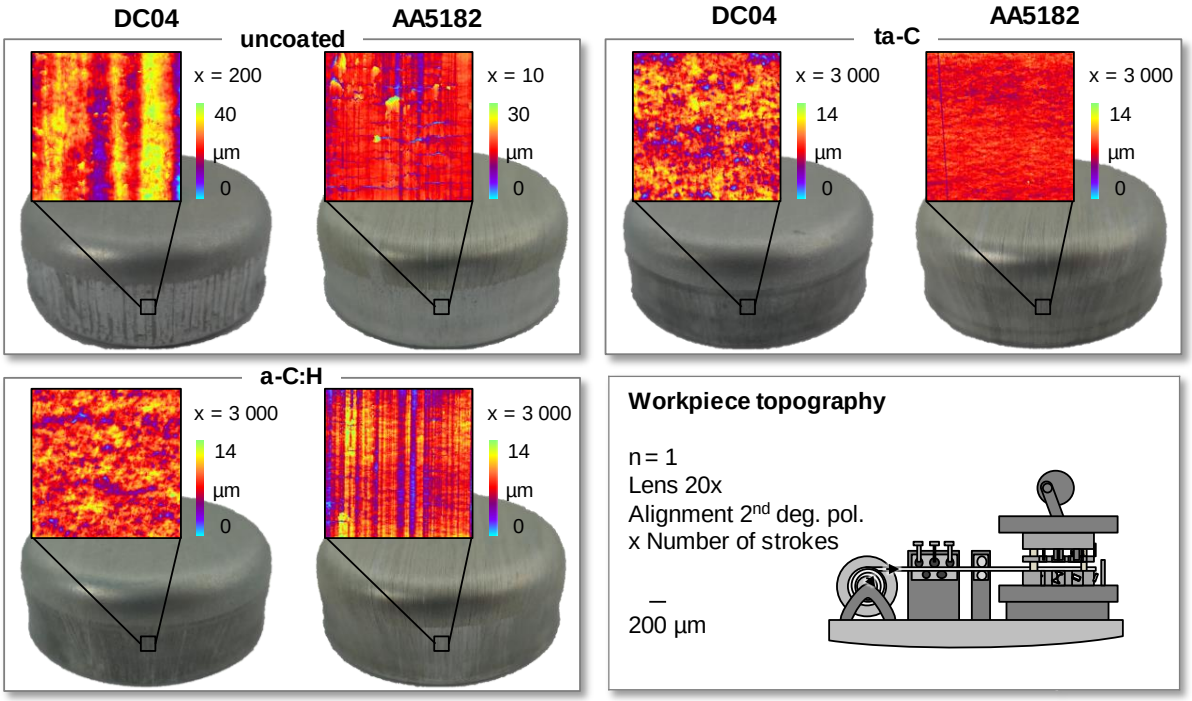

Fig. 34: Analysis of component surface quality for dry deep drawing processes

In [38] it was shown that the modifications influence the maximum forming forces due to their effect on friction. Due to this relationship, the forming force is potentially suitable for the in-situ assessment of the modification's function. Especially in dry and consequently wear-critical deep drawing processes, the monitoring of the tool condition is of particular importance. By analyzing the change in force and comparing the results with the condition of the tool surface, this target parameter is qualified for process monitoring of dry deep drawing processes. Fig. 35 shows the maximum forming forces for all wear tests. Forming with coated tools requires significantly lower forming forces than with uncoated tools. This is due to the decrease in friction and confirms the results from [20]. In addition, a lower forming force is required for forming AA5182 due to its lower yield stress (Fig. 2). For both DC04 and AA5182, as illustrated in Fig. 35 a) the forming force tends to increase with the number of components when forming with uncoated tools. This is due to the ongoing wear of the tool surfaces and the corresponding increase in friction. For all coatings, however, the forming forces decrease due to the smoothing of the tool surface during the first 50 strokes, see Fig 35 b). This is confirmed by the analysis of the tool topography (see Fig. 33) in which no wear was found when components were manufactured from DC04 and AA5182 in combination with a ta-C coating. Only for the forming of AA5182 with a-C:H coated tools the forming force increases from stroke 1 000 onwards due to the starting wear identified in Fig. 33. Thus, the potential of the maximum forming force for monitoring the tool condition in dry deep drawing processes was shown.

The wear tests proved that the modifications investigated in the laboratory tests are feasible for dry deep drawing processes. Component failure due to high friction and tool wear is prevented with the modifications for a high number of forming operations.

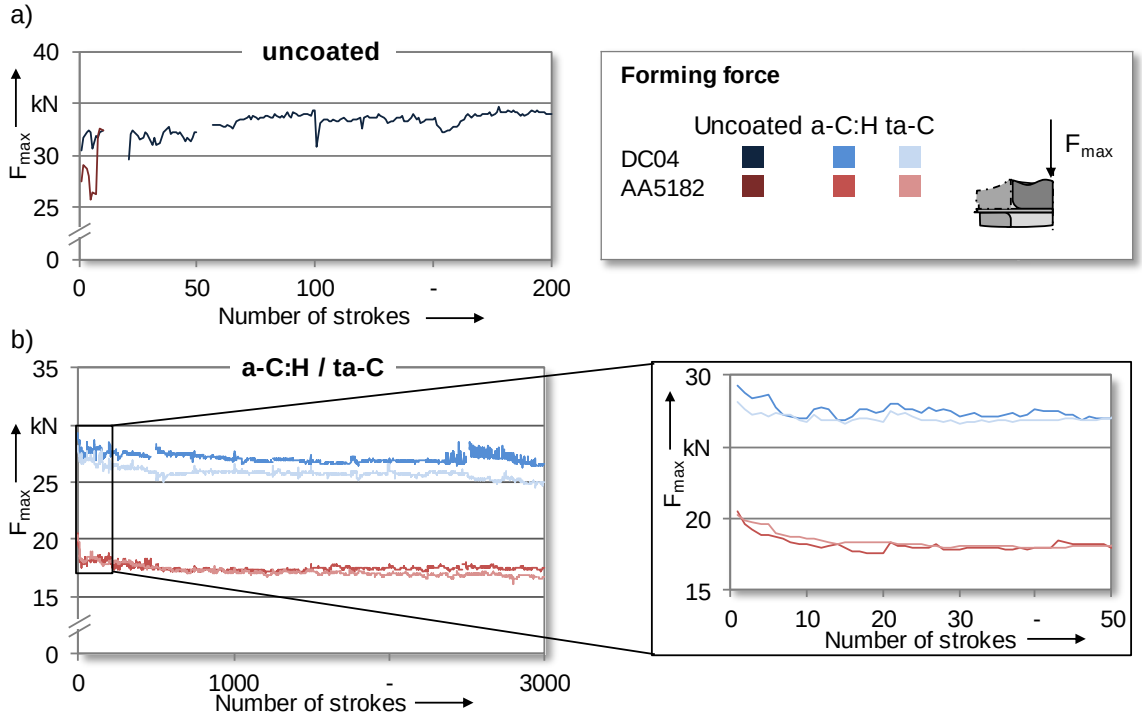

Fig. 35: Analysis of maximal forming forces for a high number of dry deep drawing processes for a) uncoated and b) coated tools

7 Summary and Conclusion

Within the scope of the presented project an increase in friction as well as adhesive wear were identified as central challenges in lubricant free deep drawing. The rise in friction was less pronounced with DC04 than with aluminum alloys, since the soft zinc coating of the DC04 has a friction-reducing effect. In section 3.3 it was shown that the strong increase in friction leads to a failure of the aluminum components by cracks, due to the local exceeding of the forming limits. Adhesive wear is critical on the one hand, as it causes a further increase in friction and, on the other hand, it worsens component quality by roughening the surface of the workpiece (section 6.2). Considering these challenges, only 200 components made of DC04 and 10 workpieces made of AA5182 could be produced with unmodified components in the forming process presented in section 6.2. In order to use the process-specific benefits of forming technology also for lubricant free processes, long tool life is required. For this reason, modifications of the tool surface to meet these challenges were investigated within the scope of the project. Different coating systems and laser-based texturing were analyzed. These are evaluated in Fig. 36 a).

a) **Central findings of laboratory test**

	Friction		Wear		Effort of modification
Material	DC04	AA5182/ AA6014	DC04	AA5182/ AA6014	
a-C:H:W smooth, mechanical polished	↑↑	↑↑↑	↑↑	↑↑↑	↑
a-C:H rough, as-deposited	↑↑↑	↑↑↑	↑↑↑	↑↑↑	↑
a-C:H smooth, mechanical polished	↓↓↓	↓↓↓	↓↓↓	↓↓	↑↑
a-C:H smooth, laser polished	↓↓↓	↓↓	0	↓	↑↑
ta-C rough, as-deposited	↑↑↑	↑↑↑	↑↑↑	↑↑↑	↑↑
ta-C smooth, mechanical polished	↓↓↓	↓↓↓	↓↓↓	↓↓↓	↑↑↑
ta-C + rectangular texture, open bottom	↓↓↓	↑↑↑	↑	↑↑	↑↑↑
ta-C + rectangular texture, closed bottom	n/a	↓	n/a	↑↑	↑↑↑

b) **Evaluation of the measures in the forming test**

	Friction		Wear		Workpiece quality		Quantity of parts	
Material	DC04	AA5182	DC04	AA5182	DC04	AA5182	DC04	AA5182
uncoated	↑↑↑	↑↑↑	↑↑	↑↑↑	↓↓↓	↓↓↓	200	10
a-C:H	↑↑↑	↑↑	↑↑↑	↑↑	↑↑↑	↑↑	> 3 000	> 3 000*
ta-C	↓↓↓	↓↓↓	↓↓↓	↓↓↓	↑↑↑	↑↑↑	> 3 000	> 3 000

* First signs of wear after 1 000 strokes

Decrease			Increase			Evaluation	
strong	medium	low	low	medium	strong	positive	negative
↓↓↓	↓↓	↓	↑	↑↑	↑↑↑		

Fig. 36: Deduction of conclusions based on a) laboratory tests and b) forming tests

Key findings regarding the coatings are that the metal dopant in the amorphous carbon network leads to high tendency of metallic adhesion on tool surface. Additionally, coatings in as-deposited state cannot be applied in tribological uses due to high roughness asperities. The post-treatment by polishing is essential and has a great impact on the tribological behavior against metal sheets. Consequently, requirements for coating for lubricant free forming are polished surfaces with as low as possible asperities and a dopant-free carbon network. Regarding the laser based texturing of tool surfaces in dry deep drawing it was found, that ultrafast laser based surface modifications have a clear influence on the tribological conditions. For example a laser based surface finishing technique was shown, which could be used to remove roughness asperities resulting from the coating process of an a-C:H coating. Compared with the conventional manual polishing, this technique is contactless, fast and suitable for automatization. Moreover, ultrafast laser texturing can be used for adjusting the friction coefficient of a coated surface on the micrometer scale. Tests with AA5182 as a sheet material led to an increased friction in and adhesion especially in the region of structure edges. Against aluminum, examined textures with closed ta-C layer at the bottom of the structures showed a slightly increased friction coefficient. Therefore, micro textures used with aluminum should not show structure edges relative to the drawing direction and have a closed coating layer even at the structure bottom to prevent adhesive wear. Additionally, the texturing process needs to prevent a sp^2 hybridization of the coating. Moreover, tests with DC04 showed that the tested geometries are able to tailor the friction coefficient in

dependence of the degree of coverage. Both, a reduction of the friction coefficient by up to 20 % in comparison with an un-textured coated surface as well as an increase of the friction coefficient can be set. Here, the reduction of the friction can be explained by a smoothing of the sheet material initiated by the increased relative contact pressure. A closed coating layer and low sp^2 hybridization is not as critical as for aluminum samples.

Based on these findings, polished a-C:H and ta-C coated tools were used for dry deep drawing of a large number of components and were evaluated in Fig. 36 b). It was proven that lubricant free deep drawing of high quantities of components made of the alloys DC04 and AA5182 can be realized with the researched modifications by avoiding adhesion and reducing friction. The modifications increase the tools life by a factor of 15 when forming DC04 and by a factor of 600 in the case of AA5182. In addition, they improve the workpiece quality by reducing the roughening of the part surface. The project has thus proven the applicability of dry deep drawing under application-oriented conditions and provided the basis for the development of dry or low-lubricated and thus environmentally friendly processes in industrial environments.

Acknowledgements

The authors thank the German Research Foundation (DFG) for supporting the presented investigations by funding the priority program SPP 1676 project ME 2043/43-1; ME 2043/50-1, ME 2043/50-2; SCHM 2115/36-1; SCHM 2115/49-1; SCHM 2115/49-2 and TR 1043/1-1; TR 1043/5-1; TR 1043/5-2 with the project title “Lubricant free forming with tailored tribological conditions”. The authors are also grateful to OTEC GmbH and H-O-T Härte- und Oberflächentechnik GmbH & Co. KG for tool polishing and coating. In addition the authors are grateful to all laboratory assistants and students who supported the execution of this study.

References

[1] F. Klocke, W. König: Fertigungsverfahren Umformen 4. Springer, Berlin, 2006
[2] K. Lange: Umformtechnik – Blechbearbeitung. Springer, Berlin, 1990
[3] F. Vollertsen, F. Schmidt: Dry Metal Forming: Definition, chances and challenges. International Journal of Precision Engineering and Manufacturing – Green Technology 1/1 (2014) 59–62
[4] A. Birkert, S. Haage, M. Straub: Umformtechnische Herstellung komplexer Karosserieteile: Auslegung von Ziehanlagen. Springer, Berlin, 2013
[5] E. Romhanji, M. M. Popović, D. M. Glišić, M. Stefanović, M. Milovanović: On the Al-Mg alloy sheets for automotive application: Problems and solutions. Metalurgija 10(3) (2004) 205–216
[6] F. Barlat, J. Brem, J. Yoon, K. Chung, R. Dick, D. Lege, F. Pourboghrat, S.-H. Choi, E. Chu: Plane stress yield function for aluminum alloy sheets–part 1: theory. International Journal of Plasticity 19 (2003) 1297–1319
[7] F. Quetting, P. Hora, K. Roll: Modelling of strain hardening behavior of sheet metals for stochastic simulations. Key Engineering Materials 504–506 (2012) 41–46
[8] K. Andreas: Einfluss der Oberflächenbeschaffenheit auf das Werkzeugeinsatzverhalten beim Kaltfließpressen. PhD-thesis, (2015)
[9] DIN 8580: Fertigungsverfahren – Begriffe, Einteilung. Beuth Verlag, Berlin, 2003
[10] H. Hetzner: Systematische Entwicklung amorpher Kohlenstoffschichten unter Berücksichtigung der Anforderungen der Blechmassivumformung. PhD-thesis, (2014)
[11] J. Shi, Z. Gong, C. Wang, B. Zhang, J. Zhang: Tribological properties of hydrogenated amorphous carbon films in different atmospheres. Diamond and Related Materials 77 (2017) 84–91
[12] J. Roberson: Diamond-like amorphous carbon. Materials Science and Engineering: R: Reports 37/4–6 (2002) 129–281
[13] H.O. Pierson: Handbook of Carbon, graphite, diamonds and fullerenes: Processing, properties and applications. Noyes Publications, New Jersey, 1993
[14] E. Doege, K.-P. Witthüser, R. Grahnert: Untersuchung der Reibungsverhältnisse beim Tiefziehen. Tribologie: Reibung, Verschleiß, Schmierung (1981) 551–575
[15] M. Merklein, M. Schmidt, S. Tremmel, S. Wartzack, K. Andreas, T. Häfner, R. Zhao, J. Tenner: Investigation of Tribological Systems for Dry Deep Drawing by Tailored Surfaces. Dry Metal Forming Open Access Journal 1 (2015) 42–56
[16] H. Freiße, S. Schmidt, T. Seefeld: Characterization of the tribological behavior of tool surfaces depending on higher contact pressures. Dry Metal Forming Open Access Journal 4 (2018) 52–58
[17] F. Zöller: Erarbeitung von Grundlagen zur Abbildung des tribologischen Systems in der Umformsimulation. PhD-thesis, (2016)
[18] J. Tenner, T. Häfner, B. Rothammer, K. Krachenfels, R. Zhao, M. Schmidt, S. Tremmel, M. Merklein: Influence of laser generated micro textured coated tool surfaces on dry deep drawing processes. Dry Metal Forming Open Access Journal 4 (2018) 35–46
[19] J. Tenner, K. Andreas, A. Radius, M. Merklein: Numerical and experimental investigation of dry deep drawing of aluminum alloys with conventional and coated tool surfaces. Procedia Engineering 207 (2017) 2245–2250
[20] J. Tenner: Realisierung schmierstofffreier Tiefziehprozesse durch maßgeschneiderte Werkzeugoberflächen. PhD-thesis, (2018)
[21] Association of German Engineers (VDI): VDI Guideline 2840. Beuth, Berlin, 2012
[22] G. Capote, G.C. Mastrapa, V.J. Trava-Airoldi: Influence of acetylene precursor diluted with argon on the microstructure and the mechanical and tribological properties of a-C:H films deposited via the modified pulsed-DC PECVD method. Surface and Coatings Technology 284 (2015) 145–152
[23] Y. Wang, Y. Ye, H. Li, L. Ji, Y. Wang, X. Liu, J. Chen, H. Zhou: Microstructure and tribological properties of the a-C:H films deposited by magnetron sputtering with CH4/Ar mixture. Surface and Coatings Technology 205/19 (2011) 4577–4581
[24] A. Mousavi, T. Kunze, T. Roch, A. Lasagni, A. Brosius: Deep drawing process without lubrication – an adapted tool for a stable, economic and environmentally friendly process. Procedia Engineering 207 (2017) 48–53

[25] DIN 4855: Kohlenstoffschichten - DLC-Schichten - Beschreibung der Schichtarchitektur. Beuth, Berlin, 2015
[26] R. Zhao, S. Tremmel: Tribologisches Einsatzverhalten von diamantähnlichen Kohlenstoffschichten (DLC) auf Werkzeugstahl gegenüber Stahl- und Aluminiumblechwerkstoffen für Trockentiefziehprozesse. In Gesellschaft für Tribologie e. V. (Eds.), 56. Tribologie-Fachtagung (pp. 25/1–25/10). (2015) Göttingen
[27] R. Zhao, J. Steiner, K. Andreas, M. Merklein, S. Tremmel: Investigation of tribological behaviour of a-C:H coatings for dry deep drawing of aluminum alloys. Tribology International 118 (2018) 484–490
[28] J. Roberson: Diamond-like amorphous carbon. Materials Science and Engineering: R: Reports 37/4–6 (2002) 129–281
[29] B. Rother, J. Vetter: Plasmabeschichtungsverfahren und Hartstoffschichten. Deutscher Verlag für Grundstoffindustrie, Leipzig, 1992
[30] B.R. Pujada, G.C.A.M. Janssen: Density, stress, hardness and reduced Young´s modulus of W-C:H coatings. Surface and Coating Technology 201 (2006) 4284–4288
[31] H.-G. Fuss, M. Frank: Industrial production of DLC coatings. In: C. Donnet, A. Erdemir, Tribology of diamond-like carbon films. Springer, New York, 2008
[32] A.C. Ferrari, J. Robertson: Interpretation of raman spectra of disordered and amorphous carbon. Physical Review B 61/20 (2000) 14095
[33] B.A. Movchan, A.V. Demchishin: Study of the structure and properties of thick condensates of nickel, titanium, tungsten, aluminum oxide and zirconium dioxide. Fiz. Metal. Metalloved 28 (1969) 653-660
[34] H.W. King, J.D. Brown, T.A. Caughlin: Temperature dependence of residual stress in TiN films on 316 stainless steel. 46 Annual Denver X-ray Conference (DXC), Denver, 1997
[35] L. Ward, F. Junge, A. Lampka, M. Dobbertin, C. Mewes, M. Wienecke: The effect of Bias Voltage and Gas Pressue on the Structure, Adhesion and Wear Behavior of Diamond Like Carbon (DLC) Coatings With Si Interlayers. Coatings 4/2 (2014) 214-230
[36] Association of German Engineers (VDI): VDI Guideline 3198. Beuth, Berlin, 1992
[37] B. Rothammer, R. Zhao, K. Krachenfels, M. Merklein: Investigation of the tribological performance of a-C:H coating systems by modifying adhesive layer for application in dry deep drawing. Proceedings of the International Tribology Conference Sendai, Sendai, 2019
[38] J. Steiner, T. Häfner, R. Zhao, K. Andreas, M. Schmidt, S. Tremmel, M. Merklein: Analysis of tool-sided surface modifications for dry deep drawing of deep drawing steel and aluminum alloys in a model process. Dry Metal Forming Open Access Journal 3 (2017) 30–40
[39] R. Woska, J. Barbehön: Metallische Adhäsion unter trockener Reibung. Zeitschrift Werkstofftechnik 13 (1982) 348–355
[40] M. Günther: Harte amorphe wasserstoffhaltige Kohlenstoffschichten mittels mittelfrequenzgepulster Plasmaentladungen: Prozesscharakterisierung und Schichteigenschaften. PhD-thesis, (2012)
[41] M. Merklein, M. Schmidt, S. Wartzack, S. Tremmel, K. Andreas, T. Häfner, R. Zhao, J. Steiner: Development and Evaluation of Tool Sided Surface modifications for Dry Deep Drawing of Steel and Aluminum Alloys. Dry Metal Forming Open Access Journal 1 (2015) 113–120
[42] B. Podgornik, J. Jerina: Surface topography effect on galling resistance of coated and uncoated tool steel. Surface and Coatings Technology 206/11–12 (2012) 2792–2800
[43] T. Häfner, B. Rothammer, J. Tenner, K. Krachenfels, M. Merklein, S. Tremmel, M. Schmidt: Adaption of tribological behavior of a-C:H coatings for application in dry deep drawing. MATEC Web of Conferences 190 (2018)
[44] T. Roch, V. Weihnacht, H.-J. Scheibe, A. Roch, A. Lasagni: Direct Laser Interference Patterning of tetrahedral amorphous carbon films for tribological applications. Diamond and Related Materials 33 (2013) 20–26
[45] T. Häfner, J. Heberle, H. Hautmann, R. Zhao, J. Tenner, S. Tremmel, M. Merklein, M. Schmidt: Effect of picosecond laser based modifications of amorphous carbon coatings on lubricant-free tribological systems. Proceedings of LPM – the 18th International Symposium on Laser Precision, 2017
[46] B.K. Tay, X. Shi, E. Liu, H.S. Tan, L.K. Cheah, H. Shi, E.C. Lim, H.Y. Lee: Tribological and optical properties of hydrogen-free Amorphous Carbon Films with Varying sp^3/sp^2 Composition. Surface and Interface Analysis 28/1 (1999) 226–230
[47] T. Häfner, J. Heberle, D. Holder, M. Schmidt: Speckle reduction techniques in holographic beam shaping for accurate and efficient picosecond laser structuring. Journal of Laser Applications 29 (2017)
[48] T. Häfner, J. Strauß, C. Roider, J. Heberle, M. Schmidt: Tailored laser beam shaping for efficient and accurate microstructuring. Applied Physics A (2018)
[49] J.W. Goodman: Some fundamental properties of speckle. Journal of the Optical Society of America 66/11 (1976) 1145–1150
[50] J. Henneberg, B. Rothammer, R. Zhao, M. Vorndran, J. Tenner, K. Krachenfels, T. Häfner, S. Tremmel, M. Schmidt, M. Merklein: Analysis of tribological behavior of surface modifications for a dry deep drawing process. Dry Metal Forming Open Access Journal 5 (2019) 13–24
[51] M. Geiger, U. Engel, M. Pfestorf: New Developments for the Qualification of Technical Surfaces in Forming Processes. Annals of the CIRP 46/1 (1997) 171–174